all mixed up

a blog

`elton/blog/blog.tex`, rev. 463: last edit by Predrag Cvitanović, 07/07/2015

Mohammad M. Farazmand, Adam Fox, John R. Elton, and Predrag Cvitanović

July 25, 2018

Contents

Chapter 4

Analyze this: John Elton land

[1]

The latest entry at the top for this blog

4.1 More stagnation point arguments

JRE July 26, 2008: Looking at the way the plane Couette symmetries act on velocity fields

$$\begin{aligned} \sigma_1\,[u,v,w](x,y,z) &= [u,v,-w](x,y,-z) \\ \sigma_2\,[u,v,w](x,y,z) &= [-u,-v,w](-x,-y,z) \\ \tau(d_x,d_z)[u,v,w](x,y,z) &= [u,v,w](x+d_x,y,z+d_z)\,. \end{aligned} \tag{4.1}$$

we see that, since τ does not affect the velocity components, the stagnation points argument will work only for the combinations of these elements which contain both σ_1 and σ_2 an odd number of times. Let us restrict ourselves to the plane Couette symmetries σ_1, σ_2, $\tau_x = \tau(L_x/2,0)$, $\tau_z = \tau(0,L_z/2)$ which generate a group of order 16. In this simplified Abelian case the requirement that permits the argument is just to have a $\sigma_1\sigma_2$ term. For this case we can write down exactly which elements permit the arguments, and the stagnation points they produce.

There are four elements of this group that contain a $\sigma_1\sigma_2$ term. These are $g_1 =$

[1] `elton/blog/EltonBlog.tex`, rev. 401: last edit by Predrag Cvitanović, 06/20/2015

$\sigma_1\sigma_2$, $g_2 = \sigma_1\sigma_2\tau_x$, $g_3 = \sigma_1\sigma_2\tau_z$, and $g_4 = \sigma_1\sigma_2\tau_x\tau_z$. [2]

$$g_1\,[u,v,w](x,y,z) = [-u,-v,-w](-x,-y,-z) \tag{4.2}$$
$$g_2\,[u,v,w](x,y,z) = [-u,-v,-w](-x+L_x/2,-y,-z) \tag{4.3}$$
$$g_3\,[u,v,w](x,y,z) = [-u,-v,-w](-x,-y,-z+L_z/2) \tag{4.4}$$
$$g_2\,[u,v,w](x,y,z) = [-u,-v,-w](-x+L_x/2,-y,-z+L_z/2) \tag{4.5}$$

Each g in turn produces four symmetrically located stagnation points in the $y = 0$ plane. Note that g_2 and g_3 are the ones which have already been discussed in sect. 4.12 and sect. 4.2.

g_1 symmetry implies that there are stagnation points at $(0,0,0)$, $(L_x/2,0,0)$, $(0,0,L_z/2)$, and $(L_x/2,0,L_z/2)$. g_2 symmetry implies that there are stagnation points at $(L_x/4,0,0)$, $(3L_x/4,0,0)$, $(L_x/4,0,L_z/2)$, and $(3L_x/4,0,L_z/2)$. g_3 symmetry implies that there are stagnation points at $(L_x/2,0,L_z/4)$, $(L_x/2,0,3L_z/4)$, $(0,0,L_z/4)$, and $(0,0,3L_z/4)$. Finally g_4 symmetry implies that there are stagnation points at $(L_x/4,0,L_z/4)$, $(L_x/4,0,3L_z/4)$, $(3L_x/4,0,L_z/4)$, and $(3L_x/4,0,3L_z/4)$. These sets of points are shown in figure 4.1.

So the question of stagnation points for a given equilibrium is, which of the g symmetries do you possess? This is a question related to invariance under the isotropy subgroups. Remember, this doesn't address the question of whether other stagnation points may exist, simply that these do or do not. For the known equilibria EQ1 - EQ11 all of them have $g3$ symmetry and EQ7, EQ8 additionally have $g2$ symmetry and that's it. Presumably this is just because searches for equilibria were done in a symmetric subspace which contained the $g3$ element (the S-symmetric subspace as it was called earlier). If equilibria are found in other subspaces that contain more g's they will have the corresponding stagnation points.

4.2 Equilibria EQ7 and EQ8

JFG July 26, 2008: n00bs.tex shows a couple equilibria in the HKW box with quarter-box shifts. It's not too deep; you just take a solution with periodicity L_x and embed it in a box of length $2L_x$. It would be better if we could devise a good notation in which the symmetries of a solution didn't depend on the box it was embedded in (i.e. were locked to the periodicity of the solution rather than the box). Maybe it would be sufficient to drop the $\tau_x^{1/2}$ shorthand in favor of the longhand $\tau(\ell_x, 0)$.

I think that for a function of fundamental wave number α (Fourier expansion $\sum_n u_n \exp(i\alpha n x)$ with at least one odd u_n nonzero), the shifts in symmetry must be limited to $\ell_x = \pi/\alpha$. Smaller shifts are not possible (for non-constant functions) and bigger ones must be integer multiples, which are equivalent to $\ell_x = \pi/\alpha$ due to periodicity. Right? I'll put pencil to paper and check.

JRE July 26, 2008 Question: "There are equilibria with other symmetries that fix x, z phase but have other translations than the half-cell shifts."

[2] JRE: I don't mean to try and introduce this as any kind of permanent notation, I just needed some way to write them down for now

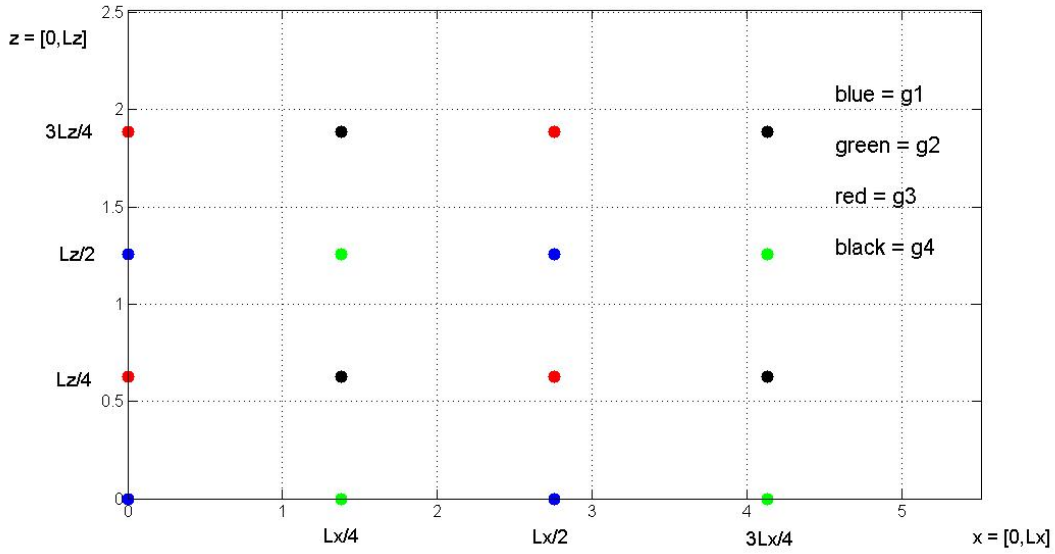

Figure 4.1: Sets of possible stagnation points. If one of the g symmetries is possessed, the velocity field will have stagnation points of the color corresponding to that g.

Other than EQ1 - EQ11? Could you tell me what these translations are, or where to look? It could help to understand the nontrivial stagnation points of EQ2.

JFG July 21, 2008: A couple comments to things stretching back a few weeks: (1) Schmiegel I group is $\{1, s_3, \tau_z, s_3\tau_z\}$ in our notation. (2) Why are most of the equilibria symmetric in the S symmetries? In a nutshell, we know that EQBs 1-8 are symmetric in $S = \{1, s_1, s_2, s_3 = s_1 s_2\}$ because they satisfy those symmetries numerically. There is no a priori reason that eqbs should be S-symmetric, other than S symmetry fixes x, z phase and so rules out relative equilibria. But s_3 symmetry alone does the same, and we have a few eqbs that have s_3 symmetry but neither s_1 nor s_2 symmetry. There are equilibria with other symmetries that fix x, z phase but have other translations than the half-cell shifts. In a rough sense, the half-cell shifts allow for the most gentle curvature in the solutions, so these will generally have lower dissipation rates, be more stable, and consequently more dynamically important than other shifts.

A bit of history will clarify. Nagata discovered the UB and LB EQBs in 1990 by continuing a known solution from Taylor-Couette flow to plane Couette. He doesn't say anything about the symmetries, but Waleffe calculated the same solutions a different way and noted that they satisfy 'shift-rotate' and 'shift-reflect' symmetry (our s_1 and s_2). We started our explorations of plane Couette dynamics around those EQBs, noted that $S = \{1, s_1, s_2, s_3 = s_1 s_2\}$ is a group and that the S-symmetric subspace was invariant under Navier-Stokes. We focused our searches for new equilibria on this subspace, since it fixes the x, z phase of solutions and since the symmetry restriction reduces the dimensionality of the eqbs' unstable manifolds. So we have found

S-symmetric eqbs primarily because we initiated our guesses within that invariant subspace. However, the subspace is unstable, and numerical simulations will creep away from it after a long time. Some of our initial guesses had sufficient deviation from the S-symmetric subspace that the Newton search was able to detect eqbs that lied close to but were not actually within that subspace. That gave us EQBs 9, 10, and 11, which are s_3 symmetric but not s_1 or s_2.

We would probably do well to look for solutions with other symmetries. Where that stands in terms of priorities, I'm not sure. It might be wise to listen to Predrag (no, I'm not kidding) and factor out the continuous symmetries beforehand, so that we don't have to conduct N different searches for N different invariant subspaces.

PC Aug 4, 2008: I need to deconstruct the s_i notation for ref. [86]. The translation table for Elton's invariance group of EQ7 and EQ8 is

$$\{s_1, \cdots, s_7\} = \{\sigma_z\tau_x, \sigma_{xy}\tau_{xz}, \sigma_{xyz}\tau_z, , \sigma_z\tau_z, \sigma_{xyz}\tau_x\tau_{xz}, \sigma_{xy}\}.$$

Using spanwise quarter-shift along z we get rid of some half-shifts

$$s_3 \to \sigma_{xyz}, s_1 \to \sigma_z\tau_{xz}, s_4 \to \sigma_z, s_5 = \sigma_{xyz}\tau_{xz},$$

so a "canonical" form of the isotropy group is

$$\begin{aligned} A_{xz} &= \{e, \sigma_{xy}, \sigma_z, \sigma_{xyz}, \tau_{xz}, \sigma_{xy}\tau_{xz}, \sigma_z\tau_{xz}, \sigma_{xyz}\tau_{xz}\} \\ &= \{e, \sigma_{xy}, \sigma_z, \sigma_{xyz}\} \times \{e, \tau_{xz}\}\,. \end{aligned} \tag{4.6}$$

According to Halcrow doctrine, factor $\{e, \tau_{xz}\}$ means that the state lives on diamond 1/2 $[L_x, L_z]$ area, tiles the cell twice.

JRE July 17, 2008: We now have the remaining two symmetries to complete the group. JFG comment: "The EQ7 and EQ8 are unique among the equilibria discussed here in that they are also symmetric under τ_{xz} as well as $s \in S$." Indeed, that is one of them, $\tau(L_x/2, L_z/2)$. The other turns out to be σ_2. Defining these to be $s_6 = \tau(L_x/2, L_z/2)$ and $s_7 = \sigma_2$ we have that $S = \{e, s_1, s_2, s_3, s_4, s_5, s_6, s_7\}$ and, as PC comments allude to, S is now a group of order 8, isomorphic to D_4.

$$s_i s_i = e \ \text{ for each element of } \ S \tag{4.7}$$
$$s_1s_2 = s_3, \ \ s_1s_3 = s_2, \ \ s_1s_4 = s_6, \ \ s_1s_5 = s_7, \ \ s_1s_6 = s_4, \ \ s_1s_7 = s_5 \tag{4.8}$$
$$s_2s_3 = s_1, \ \ s_2s_4 = s_5, \ \ s_2s_5 = s_4, \ \ s_2s_6 = s_7, \ \ s_2s_7 = s_6 \tag{4.9}$$
$$s_3s_4 = s_7, \ \ s_3s_5 = s_6, \ \ s_3s_6 = s_5, \ \ s_3s_7 = s_4 \tag{4.10}$$
$$s_4s_5 = s_2, \ \ s_4s_6 = s_1, \ \ s_4s_7 = s_3 \tag{4.11}$$
$$s_5s_6 = s_3, \ \ s_5s_7 = s_1 \tag{4.12}$$
$$s_6s_7 = s_2 \tag{4.13}$$
$$\tag{4.14}$$

PC July 16, 2008: Very nice! The perspective view of figure 4.2 is very interesting. This volume-preserving flow (area preserving in Poincaré sections) probably has invariant tori - you might be onto something there. Being quasiperiodic, they would

not be detected by your equilibria searching routines. Finding a stagnation point with purely imaginary eigenvalue would be a strong indication. So far your eigenvalues are all over the place (their inverses set dynamical time-scales, at least in neighborhoods if stagnation points), so it is hard to tell. Real part of (4.18) seems small, though.

JRE July 16, 2008: EQ7 and EQ8 possess two new symmetries that are not included in the subgroup S from sect. 4.12. These are $s_4 = \tau(0, L_z/2)\,\sigma_1$ and $s_5 = s_4 s_2$, where s_2 is the same as it was previously. These new symmetries act on velocity fields as

$$\begin{aligned} s_4\,[u,v,w](x,y,z) &= [u,v,-w](x,\ y,\ -z+L_z/2) \\ s_2\,[u,v,w](x,y,z) &= [-u,-v,w](-x+L_x/2,\ -y,\ z+L_z/2) \\ s_5\,[u,v,w](x,y,z) &= [-u,-v,-w](-x+L_x/2,\ -y,\ -z)\,. \end{aligned} \tag{4.15}$$

It can be checked that, similar to before, the set $\{e, s_4, s_2, s_5\}$ forms an Abelian group. It is not true, however, that the set $\{e, s_1, s_2, s_3, s_4, s_5\}$ which contains all of the symmetries forms a group.

PC July 16, 2008: $\{e, s_1, s_2, s_3, s_4, s_5\}$ is probably a subset of elements of a group of order 8. Presumably D_4, the product of four D_1 groups, two for refections, and two for spanwise, streamwise 1/2-cell translations, if I remember correctly. Keep multiplying, it should close. There might be equilibria hiding in this invariant subspace.

Please check **JFG May 23, 2008** discussion of Schmiegel's symmetry groups, currently section 8.22 of Halcrow blog. You might have run into a yet another symmetry subgroup, like Schmiegel's I group, but different. In halcrow/n00bsie [86] JFG writes: "EQ7 and EQ8 are S symmetric (...). They appear to be equivalent to the σ solutions from [87], where they appear to be the outer envelope in the D versus *Re* bifurcation diagram. (...). The EQ7 and EQ8 are unique among the equilibria discussed here in that they are also symmetric under τ_{xz} as well as $s \in S$."

JRE July 16, 2008: From (4.15) we also see that for EQ7 and EQ8 these symmetries imply that we will have additional stagnation points at locations where $(x, y, z) = (-x + L_x/2,\ -y,\ -z)$. This provides us with the 4 new stagnation points

$$\begin{aligned} \mathbf{x}_{\text{SP5}} &= (L_x/4, 0, 0) \\ \mathbf{x}_{\text{SP6}} &= (3L_x/4, 0, 0) \\ \mathbf{x}_{\text{SP7}} &= (L_x/4, 0, L_z/2) \\ \mathbf{x}_{\text{SP8}} &= (3L_x/4, 0, L_z/2)\,. \end{aligned} \tag{4.16}$$

Note that these stagnation points occur in pairs that are symmetric about the old stagnation points SP1-SP4, as they must by the discussion in sect. 4.3. I actually came about this in the opposite order. A Newton search on EQ8 revealed that $(L_x/4, 0, L_z/2)$ and $(3L_x/4, 0, L_z/2)$ are stagnation points. From this one may deduce that symmetry s_5 must hold, and it can then be checked that at any position the velocity field is indeed invariant under s_4 and s_5. I have checked all 11 of the equilibrium velocity fields, and curiously only EQ7 and EQ8 are invariant under these additional symmetries. Stability analysis of the new set for EQ8 gives the following.

SP5: There is one real, positive eigenvalue and a complex pair with negative real part.

$$\lambda^{(1)} = 0.03109\,, \quad \mathbf{e}^{(1)} = \begin{pmatrix} 0.85275 \\ 0.41774 \\ -0.31355 \end{pmatrix} \tag{4.17}$$

$$\{\lambda^{(2)}, \lambda^{(3)}\} = \mu^{(2)} \pm i\,\omega^{(2)} = -0.01555 \pm i\,0.59385 \tag{4.18}$$

$$\mathbf{e}^{(2)} = \begin{pmatrix} 0.24762 \\ -0.31442 \\ 0.69906 \end{pmatrix}\,, \quad \mathbf{e}^{(3)} = \begin{pmatrix} -0.20793 \\ 0.55489 \\ 0 \end{pmatrix}\,. \tag{4.19}$$

We have a 1D unstable manifold and a 2D in-spiral stable manifold. All four of the new points have the same eigenvalues. SP5 and SP8 have the same eigenvectors, as do SP6 and SP7 whose eigenvectors differ from SP5 only by the sign of the third component for $\mathbf{e}^{(1)}$ and by the sign of the first and second components for $\mathbf{e}^{(2)}$ and $\mathbf{e}^{(3)}$.

Another interesting although not necessarily useful result of numerically searching for stagnation points is the figures produced by plotting gridpoints where velocity squared is small. For a cutoff value of $\mathbf{u}^2$ which is too large to be useful for finding stagnation points we get a plot of points which has interesting and intricate patterns. figure 4.2 shows a 3D perspective view of these points, and figure 4.3 and figure 4.4 show the projection of figure 4.2 onto the xz and yz planes, respectively. Again, this is probably just more visually amusing than useful but I was surprised to see the patterns especially in figure 4.3.

PC July 11, 2008: Factorization of EQ8 SP1 and SP1 stability eigenspaces is presumably due to symmetry (4.70); spanwise z direction is $1D$ flow-invariant subspace at the stagnation points. That ensures the simplicity of the heteroclinic connection.

JRE August 12, 2008: After going through the usual techniques for EQ7 it appears that it's features are largely resemblant of EQ8. We were already aware of the eight stagnation points, and the heteroclinic connection between SP1 and SP2 appears as well. The one qualitative difference I spot is that for SP1 in the plane perpendicular to the direction of the heteroclinic connection the eigenvalues are complex, whereas for EQ8 all three were real.

JRE July 9, 2008: We will perform a similar analysis of EQ8 and EQ1 to that of the Upper Branch (EQ2). We start here with EQ8, which is a more turbulent flow with *Re* 270.

Begin once again with a cleverly chosen grid of initial trajectories to get a feel for the significant structures in the flow (this time it was clever, last time it was lucky). The grid is in a plane at $x = L_x/2$. The result, after a short integration time, is shown in figure 4.5. This perspective view already shows us quite a bit of information. Once again we have symmetries abound, as expected. The points $(L_x/2, 0, L_z/4)$ and $(L_x/2, 0, 3L_z/4)$ are stagnation points of this velocity field as well (as confirmed numerically). A shifted plot where the grid lies on the plane $x = 0$ reveals the same picture, rotated. This is to be expected (see sect. 4.2.1 below for discussion about this). Another interesting part of this plot is the four vortical structures on the left half. It may be that there are more stagnation points centered here, in any case they obviously

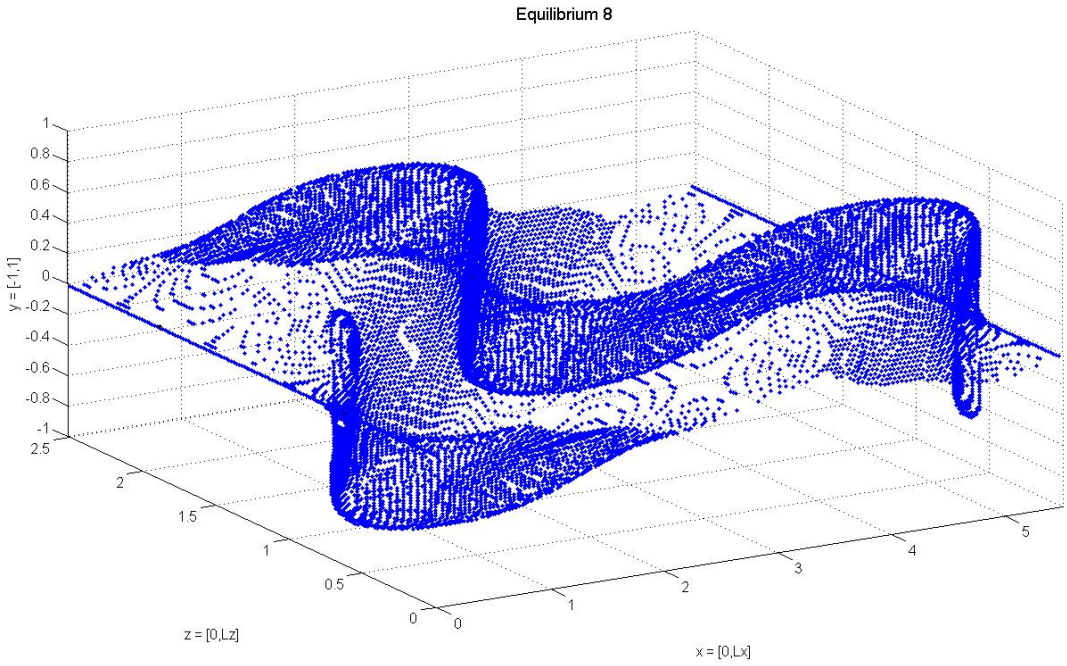

Figure 4.2: A plot of points whose value of velocity squared falls below an arbitrary cutoff of 5×10^{-7}. Perspective view.

contribute to the interesting dynamics. One final point of interest from this plot is the perfect line segment connecting the points that I was previously calling SP1 and SP2. Note that because of the finite grid size the line segment does not originate right on SP1, however other more fine plots and rotational views (not shown) make it clear that this is so. This basically already implies a heteroclinic connection between these two stagnation points. To confirm this I have computed the eigenvalues and eigenvectors of the velocity gradients matrix. For SP1 (I realize we need a different naming convention), there is indeed a real, unstable eigenvector pointing along (0,0,1) and for SP2 there is a real, stable eigenvector pointing along (0,0,1). This, together with the plot, essentially numerically proves the conjecture beyond reasonable doubt. The same result of course holds for the shifted pair at $x = 0$. The rest of the eigenvalues/eigenvectors are given below. It is interesting that for EQ8 there is a heteroclinic connection which is a perfectly horizontal line connecting the pair of trivial stagnation points in the spanwise direction, whereas for EQ2 the connection was some funny curve in the streamwise direction connected to a nontrivial stagnation point.

EQ8, SP1: There are two real, positive eigenvalues and one real, negative eigen-

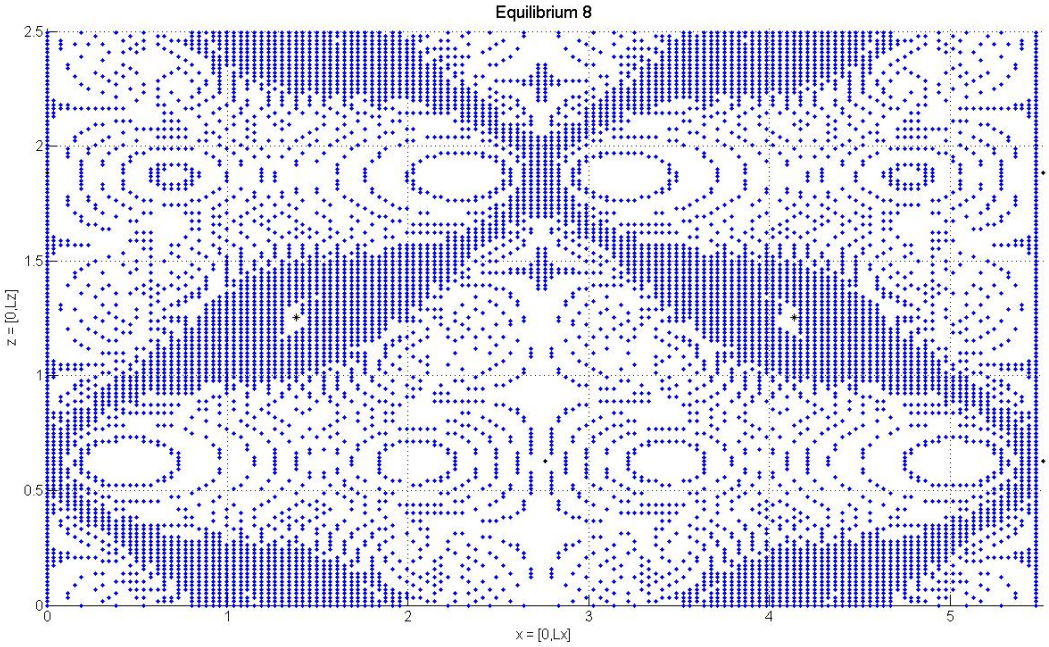

Figure 4.3: A plot of points whose value of velocity squared falls below an arbitrary cutoff of 5×10^{-7}. Projection onto the xz plane.

value. [3]

$$\begin{aligned} \left(\lambda^{(1)}, \lambda^{(2)}, \lambda^{(3)}\right) &= (0.363557, 0.227831, -0.591389) \\ \left(\mathbf{e}^{(1)}, \mathbf{e}^{(2)}, \mathbf{e}^{(3)}\right) &= \left(\begin{pmatrix} 0 \\ 0 \\ 1 \end{pmatrix}, \begin{pmatrix} -0.733415 \\ -0.679780 \\ 0 \end{pmatrix}, \begin{pmatrix} 0.991005 \\ 0.133824 \\ 0 \end{pmatrix} \right) . \end{aligned} \tag{4.20}$$

EQ8, SP2: There are two real, positive eigenvalues and one real, negative eigenvalue.

$$\begin{aligned} \left(\lambda^{(1)}, \lambda^{(2)}, \lambda^{(3)}\right) &= (0.992857, 0.255973, -1.248830) \\ \left(\mathbf{e}^{(1)}, \mathbf{e}^{(2)}, \mathbf{e}^{(3)}\right) &= \left(\begin{pmatrix} 0.116961 \\ -0.993136 \\ 0 \end{pmatrix}, \begin{pmatrix} 0.957795 \\ 0.287450 \\ 0 \end{pmatrix}, \begin{pmatrix} 0 \\ 0 \\ 1 \end{pmatrix} \right) . \end{aligned} \tag{4.21}$$

[3] Predrag: reordered eigenvalues by their magnitude

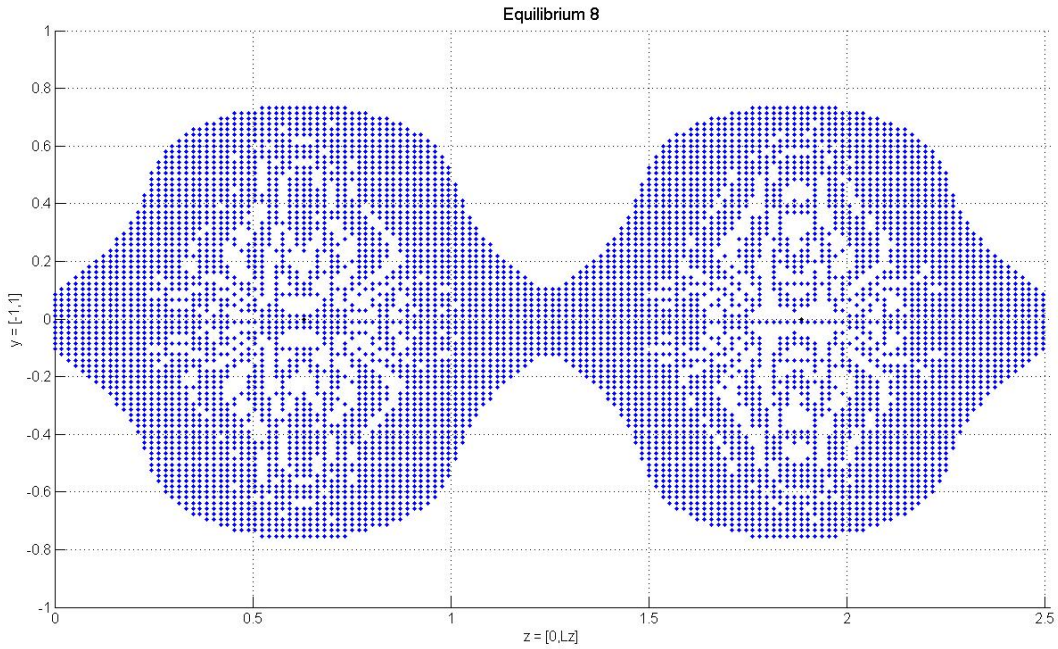

Figure 4.4: A plot of points whose value of velocity squared falls below an arbitrary cutoff of 5×10^{-7}. Projection onto the yz plane.

4.2.1 Question on symmetries

I have confirmed for myself that the Navier-Stokes equations are invariant for any symmetry in the group generated by σ_1, σ_2, τ. What I'm not clear on is the following: In sect. 4.12 it is stated that "Most of the Eulerian equilibria that we know of so far are invariant under the 'shift-reflect' symmetry $s_1 = \tau(L_x/2, 0)\,\sigma_1$ and the 'shift-rotate' symmetry $s_2 = \tau(L_x/z, L_z/2)\,\sigma_2$. These symmetries form a subgroup $S = \{1, s_1, s_2, s_3\}$, $s_3 = s_1 s_2$, which is isomorphic to the Abelian dihedral group D_2". First, I would like to ask how this is known. Is there a theoretical argument for it, or is it simply known empirically? From my numerical work it is certainly seen to be true, ii is just not yet clear to me why, from first principles, that this is so. Also, I should ask to confirm that it is known to be true for EQ1 and EQ8, although I have already basically shown it for EQ8.

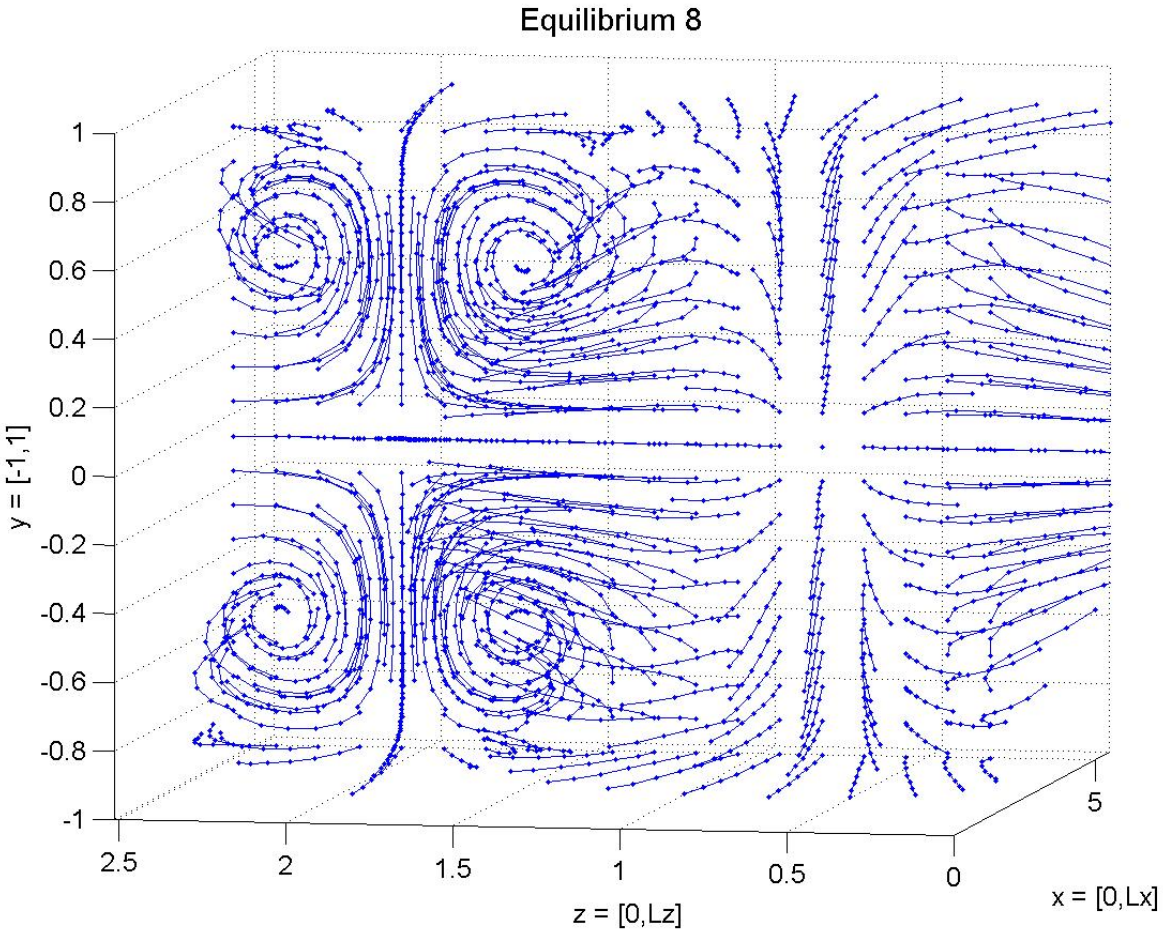

Figure 4.5: A grid of initial trajectories in the plane $x = L_x/2$ integrated for short time.

4.3 Proof that any new stagnation point must have a partner lying on a line through an oldie (SP1-SP4), equidistant.

JRE June 10, 2008: This basically follows from the action of $s3 \in S$ on velocity fields (sect. 4.12),

$$s_3\,[u,v,w](x,y,z) = [-u,-v,-w](-x,\,-y,\,-z+L_z/2)\,.$$

If $(x_{\rm SP}, y_{\rm SP}, z_{\rm SP})$ is a stagnation point, $[u,v,w](x_{\rm SP}, y_{\rm SP}, z_{\rm SP}) = [0,0,0]$, then

$$\begin{aligned} s_3\,[u,v,w](x_{\rm SP}, y_{\rm SP}, z_{\rm SP}) &= [-u,-v,-w](-x_{\rm SP},\, -y_{\rm SP},\, -z_{\rm SP}+L_z/2) \\ &= [0,0,0](-x_{\rm SP},\, -y_{\rm SP},\, -z_{\rm SP}+L_z/2). \end{aligned} \tag{4.22}$$

So $\mathbf{x}_{\rm SP'} = (-x_{\rm SP},\, -y_{\rm SP},\, -z_{\rm SP}+L_z/2)$ is also a stagnation point.
We may parameterize a line passing through two points x_1, x_2 as

$$x = x_1 + (x_2 - x_1)t \tag{4.23}$$
$$y = y_1 + (y_2 - y_1)t \tag{4.24}$$
$$z = z_1 + (z_2 - z_1)t \tag{4.25}$$
$$t \in (-\infty, \infty) \tag{4.26}$$

For the case above this becomes

$$x = x_{\rm SP}(1-2t) \tag{4.27}$$
$$y = y_{\rm SP}(1-2t) \tag{4.28}$$
$$z = z_{\rm SP}(1-2t) + \frac{L_z}{2}t \tag{4.29}$$

When $t = 1/2$ this system returns $(x,y,z) = (0,0,L_z/4)$, showing that SP3 lies on the line between these two stagnation points and is halfway in between them.

If we invoke the box periodicities: $x = x + L_x$, $z = z + L_z$, we can show that the pair of fixed points is symmetric about any of the other SP1-SP4.

$\mathbf{x} = \mathbf{x} + \mathbf{L_x}$:
$(x_{\rm SP}, y_{\rm SP}, z_{\rm SP})$ a stagnation point $\Rightarrow (-x_{\rm SP}+L_x, -y_{\rm SP}, z_{\rm SP}+L_z/2)$ a stagnation point.

$$x = x_{\rm SP}(1-2t) + L_x t \tag{4.30}$$
$$y = y_{\rm SP}(1-2t) \tag{4.31}$$
$$z = z_{\rm SP}(1-2t) + \frac{L_z}{2}t \tag{4.32}$$

When $t = 1/2$ this returns $(x,y,z) = (L_x/2, 0, L_z/4)$ so that the points lie symmetrically on a line passing through SP1.

$\mathbf{z} = \mathbf{z} + \mathbf{L_z}$:
$(x_{\rm SP}, y_{\rm SP}, z_{\rm SP})$ a stagnation point $\Rightarrow (-x_{\rm SP}, -y_{\rm SP}, z_{\rm SP}+3L_z/2)$ a stagnation point.

$$x = x_{\rm SP}(1-2t) \tag{4.33}$$
$$y = y_{\rm SP}(1-2t) \tag{4.34}$$
$$z = z_{\rm SP}(1-2t) + 3\frac{L_z}{2}t \tag{4.35}$$

When $t = 1/2$ this returns $(x,y,z) = (0,0,3L_z/4)$ so that the points lie symmetrically on a line passing through SP4. And finally,

$\mathbf{z} = \mathbf{z} + \mathbf{L_z}, \mathbf{x} = \mathbf{x} + \mathbf{L_x}$:
$(x_{\rm SP}, y_{\rm SP}, z_{\rm SP})$ a stagnation point $\Rightarrow (-x_{\rm SP}+L_x, -y_{\rm SP}, z_{\rm SP}+3L_z/2)$ a stagnation point.

$$x = x_{\rm SP}(1-2t) + L_x t \tag{4.36}$$
$$y = y_{\rm SP}(1-2t) \tag{4.37}$$
$$z = z_{\rm SP}(1-2t) + 3\frac{L_z}{2}t \tag{4.38}$$

When $t = 1/2$ this returns $(x, y, z) = (L_x/2, 0, 3L_z/4)$ so that the points lie symmetrically on a line passing through SP2.

This pairwise symmetric requirement for stagnation points is nice, but still there is the deeper question of, should any exist at all? I haven't been able to answer this yet, but a possible line of reasoning is the following: Any stagnation point occurs at the intersection of the three surfaces $u = 0$, $v = 0$, $w = 0$. We know these three surfaces intersect at the four points SP1-SP4. Given that they are smooth, we might be able to come up with some kind of argument that shows that in fact these surfaces then *must* intersect somewhere else. It's a thought anyway.

4.4 A colorful physical space portrait of the Upper Branch

JRE June 04, 2008: With a much faster interpolater and some improved plotting techniques, I have produced a picture of the dynamical behavior between our known stagnation points.

First, in figure 4.6, I have attempted to give a clear label of where these points lie within one periodic interval. SP1 through SP4 lie in the plane $y = 0$. SP5 and SP6 are symmetric about SP1. Note that a translation of SP6 would also lie in this box as well, situated below SP4, but I have chosen to omit it from this picture. At certain times it will be convenient to picture slightly different translations of these points than as they appear in figure 4.6.

The interesting dynamics and connections between the different stagnation points occur along the x direction. To understand what is happening one needs to look only at a subset of these stagnation points that lies in the right or left half of the box, that is, in the interval $[0, L_z/2]$ or the interval $[L_z/2, L_z]$. I have chosen to give results for the points lying in the interval $[0, L_z/2]$. In the x direction the most convenient interval is not actually $[0, L_x]$. I have chosen to look at the stagnation points in the open interval $(-L_x/2, L_x)$, open so as to ignore the repeated translations on the boundary. Thus the domain of investigation is

$$\Omega = (-L_x/2, L_x) \times [-1, 1] \times [0, L_z/2] \tag{4.39}$$

Within this domain there are four stagnation points. They are SP1, SP3, SP5, and SP6. In figure 4.7 I show these four points in Ω. Note that SP6 is a translated version from the way it was viewed in figure 4.6. The reason for this will soon be clear.

I will start by discussing the most interesting result, the heteroclinic connections between SP5 and SP3, and similarly between SP6 and SP3. The picture is figure 4.8.

These surfaces have kind of an eerie beauty. The red curves are the 1D unstable manifolds of SP5 and SP6, or equivalently the stable manifold of SP3. Their thick appearance is simply so that they can be seen within the blue surface. They are actually just a single trajectory. The blue surface, the unstable manifold of SP3, is found in the following way. A large number of initial conditions very close to SP3 (in the plane of it's unstable eigenvectors) are evolved forward in time. Because the integration always breaks down as these trajectories get near to SP5 and SP6, in practice I also plot the stable manifolds of SP5 and SP6 and connect them with the unstable manifold of SP3 in the middle region, where they are both accurate.

We now bring SP1 into the picture. SP1 has a 2D unstable manifold and a 1D stable manifold. The result of all of these manifolds plotted together is figure 4.9. The relation of the stable manifold (yellow curve) and unstable manifold (green surface) of SP1 to the blue surface is quite interesting. These trajectories tightly hug the blue surface as they spiral around it.

One merely translates the image in figure 4.9 in the x direction by an amount L_x to give a complete picture in any periodic cell. The same picture will also occur symmetrically (translated by $L_x/2$ and $L_z/2$) in the left half of the box.

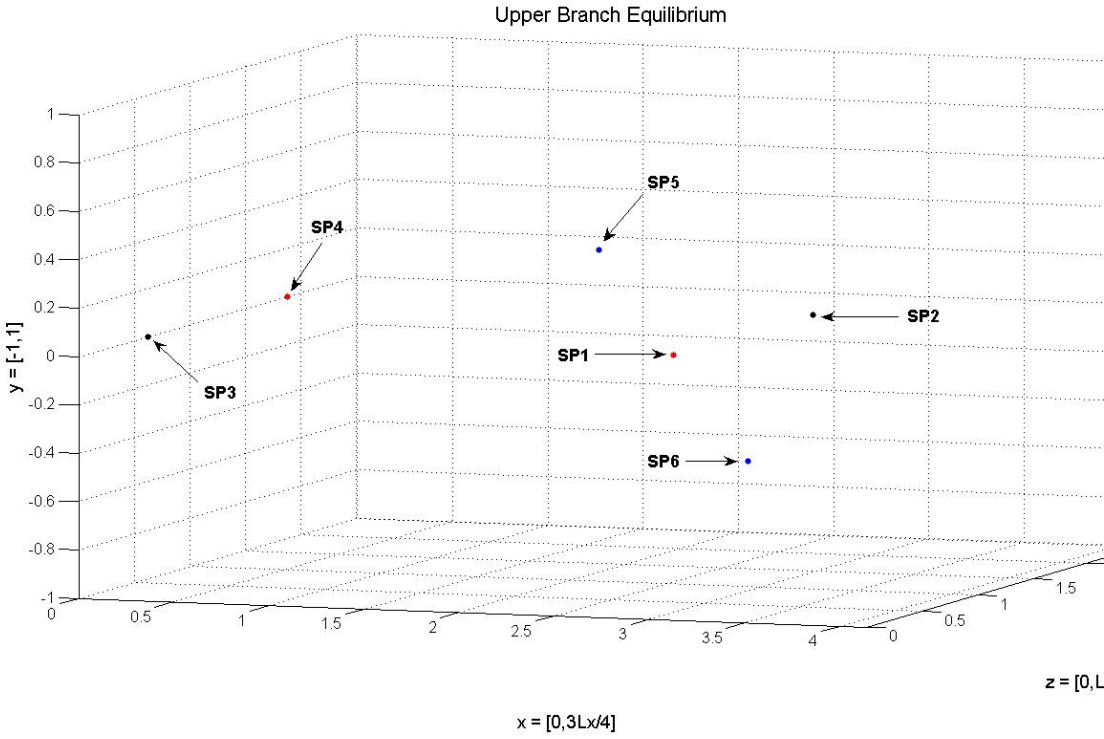

Figure 4.6: The 6 known unique stagnation points within one periodic box, SP1 through SP6. The pair SP1 and SP4 are related through a symmetry, and similarly for the pairs SP2 with SP3, and SP5 with SP6.

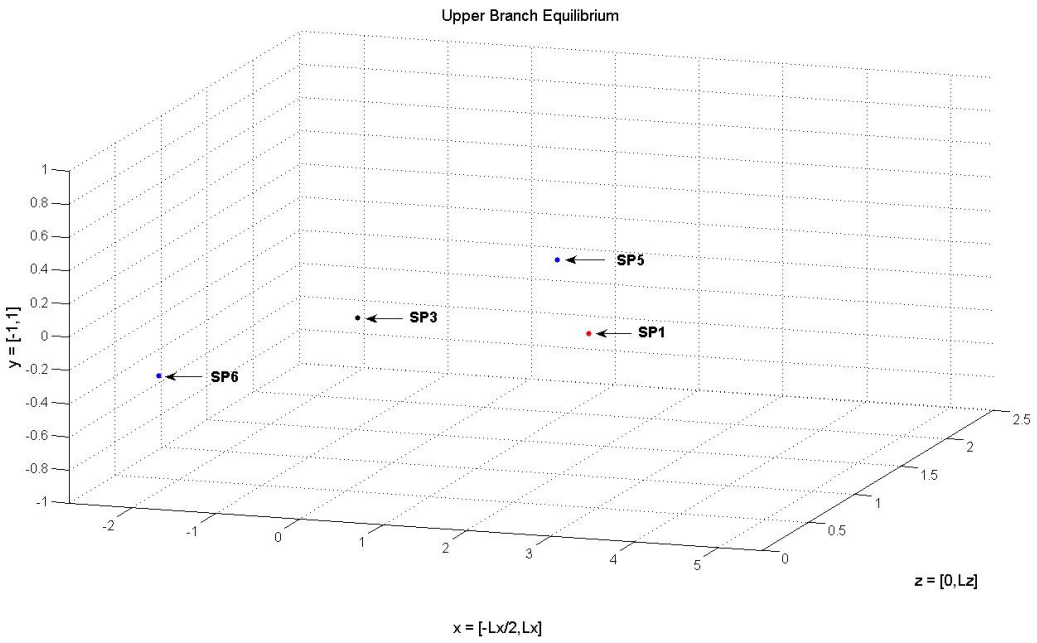

Figure 4.7: The 4 stagnation points that occur within the domain Ω.

4.5 The Navier-Stokes equations

JRE May 27, 2008: The underlying equations that govern the motion of plane Couette flow are of course the Navier-Stokes equations, along with boundary conditions. The boundary conditions in the x and z directions are periodic, $\mathbf{u}(x,y,z) = \mathbf{u}(x + L_x, y, z) = \mathbf{u}(x, y, z + L_z)$. In the y direction, $\mathbf{u} = (1,0,0)$ at $\mathbf{x} = (0,1,0)$ and $\mathbf{u} = (-1,0,0)$ at $\mathbf{x} = (0,-1,0)$.

The fluid is taken to be incompressible, so in this case the Navier-Stokes equations are

$$\frac{\partial \mathbf{u}}{\partial t} + (\mathbf{u}\cdot\nabla)\mathbf{u} = -\nabla p + \nu\nabla^2\mathbf{u}\,, \qquad \nabla\cdot\mathbf{u} = 0\,. \tag{4.40}$$

As far as I know these are all of the conditions and assumptions that are made. I would first like to confirm that this is correct, that (4.40) is the exact form of the Navier-Stokes equations that are being used for plane Couette flow.

The starting point for everything that I have been doing so far is to load the spectral coefficients, $\hat{\mathbf{u}}_{m_x,m_y,m_z}$, from (7.1). From my perspective these coefficients are kind of a magical data set that allows me to correctly compute velocities, but of course I know they came from a DNS integration of (4.40), namely through Channelflow.

For the Upper Branch equilibrium that I have been working with, (4.40) simplifies to

$$(\mathbf{u}\cdot\nabla)\mathbf{u} = -\nabla p + \nu\nabla^2\mathbf{u}\,, \tag{4.41}$$

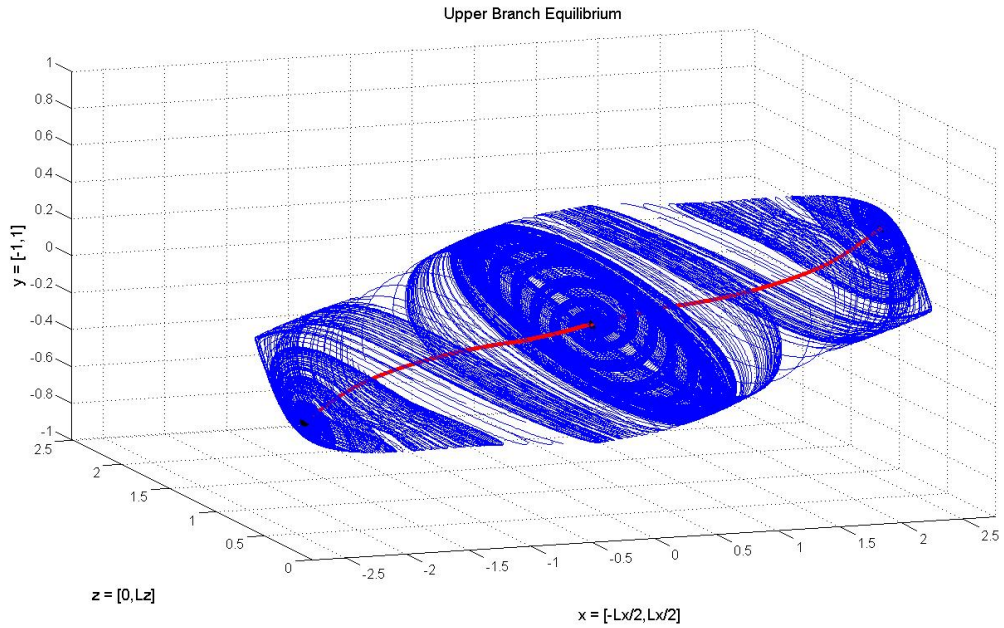

Figure 4.8: Heteroclinic pairs.

and the only other thing I know about it is that $Re = 400$. I would prefer to know the exact value of ν since it is the fundamental parameter in (4.41). Since

$$Re = \frac{\overline{u}L}{\nu} \tag{4.42}$$

where $\overline{u}$ is the average fluid velocity and L is the characteristic length, this amounts to asking what values are taken for $\overline{u}$ and L? Or maybe someone already knows and can tell me what ν is for this particular box at $Re = 400$. Interestingly, since I can compute $\mathbf{u}$, $\nabla\mathbf{u}$, and $\nabla^2\mathbf{u}$, as a crosscheck I could compute ν directly by taking the curl of both sides of (4.41).

At a stagnation point of an equilibrium velocity field the Navier-Stokes equations (4.41) simplify further. At a point where $\mathbf{u} = 0$, it is certainly true that

$$\nu\nabla^2\mathbf{u} = -\nabla p, \tag{4.43}$$

and I think that this is probably a sufficient condition to specify a stagnation point, for the following reason.

When $(\mathbf{u}\cdot\nabla)\mathbf{u}$ is written out in component form we see that it is the vector

$$\begin{pmatrix} u\frac{\partial u}{\partial x} + v\frac{\partial u}{\partial y} + w\frac{\partial u}{\partial z} \\ u\frac{\partial v}{\partial x} + v\frac{\partial v}{\partial y} + w\frac{\partial v}{\partial z} \\ u\frac{\partial w}{\partial x} + v\frac{\partial w}{\partial y} + w\frac{\partial w}{\partial z} \end{pmatrix} = \begin{pmatrix} \frac{\partial u}{\partial x} & \frac{\partial u}{\partial y} & \frac{\partial u}{\partial z} \\ \frac{\partial v}{\partial x} & \frac{\partial v}{\partial y} & \frac{\partial v}{\partial z} \\ \frac{\partial w}{\partial x} & \frac{\partial w}{\partial y} & \frac{\partial w}{\partial z} \end{pmatrix} \begin{pmatrix} u \\ v \\ w \end{pmatrix} = A\mathbf{u} \tag{4.44}$$

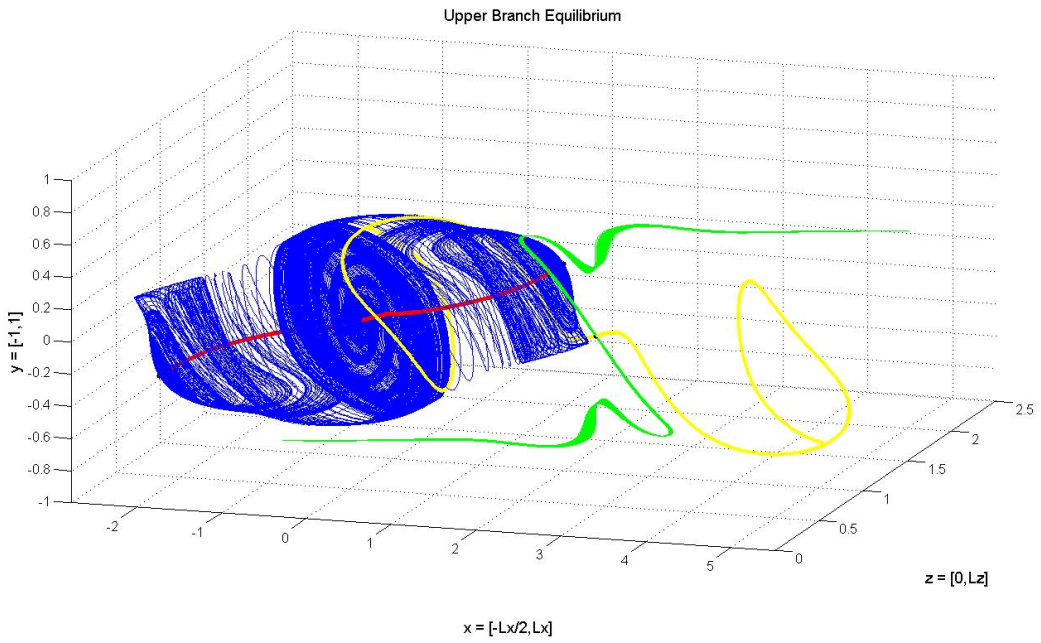

Figure 4.9: Full physical space relations between the stagnation points.

where A is the velocity gradients matrix. So if (4.43) holds then $A\mathbf{u} = 0$ and this implies we are at a stagnation point unless the nullspace of A is nontrivial. This can only happen if the three velocity gradients in A are co-planar. This seems unlikely, and there may be a physical reason that proves it can't ever happen. So that's why I say I think (4.43) is a sufficient condition for specifying a stagnation point. It's simplified form may give insight into solutions or symmetries for stagnation points.

JFG May 29, 2008: In most of our work (and in channelflow) $\mathbf{u}$ represents the *difference* from the laminar flow. I'll get to that in a minute, but first I'll do the nondimensionalization to address the ν vs Re issue. Start with Navier-Stokes on the total fluid velocity field $\mathbf{u_{tot}}$

$$\frac{\partial \mathbf{u_{tot}}}{\partial t} + \mathbf{u_{tot}} \cdot \nabla \mathbf{u_{tot}} = -\nabla p + \nu \nabla^2 \mathbf{u_{tot}}\,, \quad \nabla \cdot \mathbf{u_{tot}} = 0 \tag{4.45}$$

and boundary conditions $\mathbf{u_{tot}} = \pm U$ at $y = \pm L$. Rescale variables: $y \to y/L$, (same for x, z), $u \to u/U$, $t \to (U/L)\,t$, and $p \to U^2 p$. That gives

$$\frac{\partial \mathbf{u_{tot}}}{\partial t} + \mathbf{u_{tot}} \cdot \nabla \mathbf{u_{tot}} = -\nabla p + \frac{1}{Re} \nabla^2 \mathbf{u_{tot}}\,, \quad \nabla \cdot \mathbf{u_{tot}} = 0, \tag{4.46}$$

where $Re = UL/\nu$, and boundary conditions $\mathbf{u_{tot}} = \pm 1\hat{\mathbf{x}}$ at $y = \pm 1$. This is the nondimensionalized Navier-Stokes equation. You can think of the nondimensionalized

equations as having length scale $L = 1$, velocity scale $U = 1$, and viscosity $\nu = 1/Re$, or better, the nondimensional parameter $1/Re$ replacing viscosity.

Now break up the total velocity field into two components: $\mathbf{u_{tot}} = y\hat{\mathbf{x}} + \mathbf{u}$. Here $y\hat{\mathbf{x}}$ is the laminar velocity field and $\mathbf{u}$ is the difference between the total velocity and laminar. Substitute $y\hat{\mathbf{x}}+\mathbf{u}$ for $\mathbf{u_{tot}}$ in the nondimensionalized Navier-Stokes equations to get

$$\frac{\partial \mathbf{u}}{\partial t} + y\frac{\partial \mathbf{u}}{\partial x} + v\,\hat{\mathbf{x}} + \mathbf{u}\cdot\nabla\mathbf{u} = -\nabla p + \frac{1}{Re}\nabla^2\mathbf{u}\,, \quad \nabla\cdot\mathbf{u} = 0 \tag{4.47}$$

and boundary conditions $\mathbf{u} = 0$ at $y \pm 1$.

The equilibrium fields such as EQ2 satisfy (4.47). [4] This equation is a little more complicated than (4.46), but having Dirichlet boundary conditions on $\mathbf{u}$ makes analysis much easier, since the set of allowable $\mathbf{u}$ form a vector space. The set of allowable $\mathbf{u_{tot}}$ doesn't, since the sum of two allowable $\mathbf{u_{tot}}$ generally does not satisfy the boundary condition $\mathbf{u_{tot}} = \pm 1$ at $y \pm 1$. By "allowable" I mean those fields that satisfy incompressibility and boundary conditions.

So, in a nutshell, (1) the equilibrium fields satisfy (4.47), and (2) you don't need ν, you need $1/Re$.

Ok, that is just an explanation of our conventions, so that we're all on the same page. Your larger issues stand, keeping in mind that they apply to what we call $\mathbf{u_{tot}}$. But note how these issues play out for the laminar solution. For $\mathbf{u_{tot}} = y\hat{\mathbf{x}}$, each of the terms $1/Re\,\nabla^2\mathbf{u_{tot}}$, ∇p, and $\mathbf{u_{tot}}\cdot\nabla\mathbf{u_{tot}}$ is identically zero throughout the flow domain (in fact we obtain $\nabla p = 0$ from the other two identities.) But stagnation points are limited to the plane $y = 0$. So there are situations in which the null space of $\mathbf{u_{tot}}\cdot\nabla$ is nontrivial, and $1/Re\,\nabla^2\mathbf{u_{tot}} = -\nabla p$, does not imply stagnation.

JRE May 29, 2008: Laminar example is a nice proof that it can in fact happen that $1/Re\,\nabla^2\mathbf{u_{tot}} = -\nabla p$ does not imply stagnation, in this case because two of the velocity gradients in A are identically zero. It still seems that in general for a typical velocity field there is no reason to expect that the three velocity gradients would lie in the same plane, so maybe we could say that $1/Re\,\nabla^2\mathbf{u_{tot}} = -\nabla p$ implies stagnation, almost always?

4.6 New stagnation points

JRE May 23, 2008: Starting from the gridpoint value (4.55) with smallest velocity in the suspicious region, $\mathbf{x}_0 = (2.33476, 0.40952, 0.64577)$, and its reflection through $\mathbf{x}_{\text{SP1}}$, $\mathbf{x}_0' = 2\mathbf{x}_{\text{SP1}} - \mathbf{x}_0$, the Newton iteration

$$\mathbf{x}_{k+1} = \mathbf{x}_k - A^{-1}(\mathbf{x}_k)\,\mathbf{u}(\mathbf{x}_k) \tag{4.48}$$

[4] JRE: Just to be completely clear, should we say the equilibrium fields such as EQ2 satisfy (4.47), but with the $\frac{\partial \mathbf{u}}{\partial t}$ term set to 0?

converged rapidly to the new pair of stagnation points, accurate to $\approx 10^{-16}$: [5]

$$\mathbf{x}_{\text{SP5}} = (2.35105561774981, 0.42293662349708, 0.65200166068573) \tag{4.49}$$

$$\mathbf{x}_{\text{SP6}} = (3.16051044117966, -0.42293662349708, 0.60463540075018)\,. \tag{4.50}$$

We see the symmetry in the y-component of this pair, as was expected looking at figure 4.13. These points are symmetric about the point SP1 in all three dimensions,

$$(\mathbf{x}_{\text{SP5}} + \mathbf{x}_{\text{SP6}})/2 = \mathbf{x}_{\text{SP1}}\,. \tag{4.51}$$

It would be nice if we could think of a symmetry argument for their existence. However, unlike (4.73) their components have no rational relation to L_x, L_z, so these are nontrivial stagnation points.

Stagnation points SP5, SP6: There is one real, positive eigenvalue and a complex pair with negative real part. [6]

$$\lambda^{(1)} = 0.1453207\,, \quad \mathbf{e}^{(1)} = \begin{pmatrix} 0.9307982 \\ 0.3502306 \\ 0.1046576 \end{pmatrix} \tag{4.52}$$

$$\{\lambda^{(2)}, \lambda^{(3)}\} = \mu^{(2)} \pm i\,\omega^{(2)} = -0.0726603 \pm i\,0.3733478$$

$$\mathbf{e}^{(2)} = \begin{pmatrix} 0.5226203 \\ -0.6703938 \\ 0.2065610 \end{pmatrix}\,, \quad \mathbf{e}^{(3)} = \begin{pmatrix} 0.3779843 \\ 0 \\ -0.3031510 \end{pmatrix}\,. \tag{4.53}$$

The velocity gradients matrix is

$$A = \begin{pmatrix} 0.0225166 & 0.0985763 & 0.7623083 \\ 0.1714566 & -0.1275193 & -0.6118476 \\ -0.0615378 & 0.1755954 & 0.1050028 \end{pmatrix}\,. \tag{4.54}$$

We have this time a 1D unstable manifold and a 2D in-spiral stable manifold.

I have been labeling stagnation points to include all of the points which are inside a single periodic cell. However even within this cell there is a redundancy in labeling all of these points as distinct. There are really *three* distinct stagnation points in the fundamental domain and the rest result from invariance under $\mathbf{S}$ and should really be quotiented out. The dynamics between these three stagnation points and there translates is quite interesting. I began discussing possible heteroclinic connections in sect. 4.7, and looking at figure 4.10 it is now strongly suggestive that there exists a SP5 $\to$ SP4 heteroclinic connection. The red curve is the stable manifold of SP4. The blue curve is the unstable manifold of the new SP5. I suspect that with a perfect integration these are one in the same.

A complete phase space portrait (ignoring periodic orbits for the moment) should be coming soon. It looks like we have all of the stagnation points, and short of some

[5] Predrag: experimenting with upper case vs lower case for SP1. Will settle on preferred notation later.

[6] Predrag: always write eigenvectors. I replaced these:

$$\mathbf{e}^{(2)} = \begin{pmatrix} 0.5226203 - 0.3779843i \\ -0.6703938 \\ 0.2065610 + 0.3031510i \end{pmatrix}\,, \quad \mathbf{e}^{(3)} = \begin{pmatrix} 0.5226203 + 0.3779843i \\ -0.6703938 \\ 0.2065610 - 0.3031510i \end{pmatrix}\,.$$

numerical difficulties with plotting the stable and unstable manifolds we have a pretty good understanding of the interesting heteroclinic ménage à trois that is occurring between our three distinct stagnation points. [7]

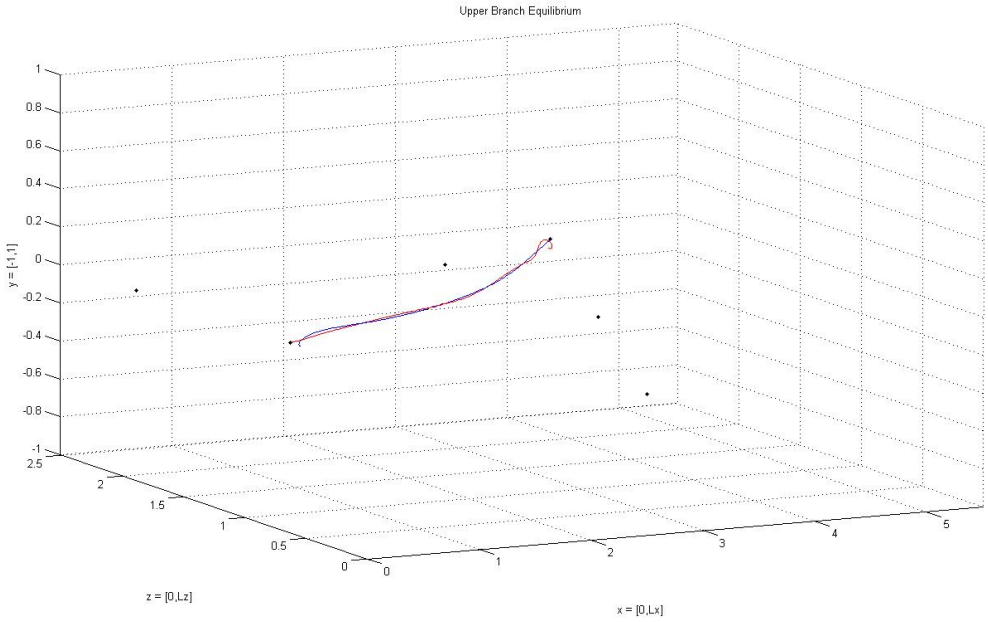

Figure 4.10: Stable manifold of SP4 (red curve) and unstable manifold of SP5 (blue curve). These are presumably the same and form a SP5 $\rightarrow$ SP4 heteroclinic connection.

4.7 Possible heteroclinic connections and evidence of a new pair of stagnation points

JRE May 21, 2008: Of the four known stagnation points it appears that there may be a heteroclinic connection between the two pairs of qualitatively different points.

Possibly heteroclinically connected pairs are SP1 $\rightarrow$ SP3 and SP2 $\rightarrow$ SP4, and the behavior for each pair is the same except that one pair is shifted by $L_x/2$ from the other pair, so really there is only pair of points to consider and the behavior of the other pair will mimic the first. The pairing occurs streamwise rather than spanwise. As in sect. 4.8, local stability analysis shows that SP1 has all real eigenvalues with a 1D stable manifold, and a 2D unstable manifold which is locally a plane. SP3 has a 2D unstable manifold with complex eigenvalues which spiral out in a plane and a 1D stable manifold. Computing these manifolds numerically beyond the linear regime

[7] Predrag: In all figures: can you add a subroutine that plots all stagnation points, labeled

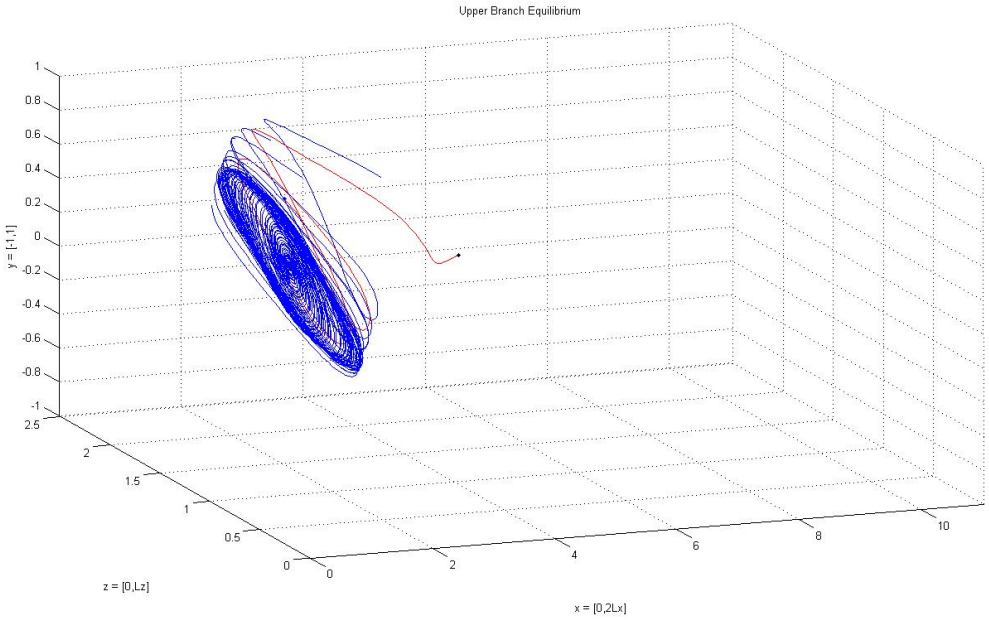

Figure 4.11: Stable manifold of SP4 (red curve) and unstable manifold of SP2 (blue surface)

shows that there 'might' exist heteroclinic connection between this pair (and likewise the other pair SP2 and SP4). Unfortunately I do not yet see an analytical argument for why this should or should not exist. Since the pairing is between stagnation points of a qualitatively different nature (not just eigenvalues sign-flipped) a time reversal argument does not imply the connection. It is still certainly possible that there are other symmetries of plane Couette flow which I have not considered that might imply a connection.

To be more specific about "there 'might' exist heteroclinic connections," refer to figure 4.11. We see the stable manifold of SP4 (red curve) and the unstable manifold of SP2 (blue surface). The stable manifold of SP4 is computed by starting a trajectory along the stable eigenvector very close to the stagnation point and integrating backwards in time. The unstable manifold of SP2 is computed by starting many trajectories in the plane spanned by the real and imaginary parts of the unstable complex eigenvectors and integrating them forward in time. I am using the exact sum to give the velocity field at each step rather than the interpolation method in order to assure greatest accuracy. We see that as the unstable manifold evolves the initial plane begins to tilt and trajectories eventually start to spread out along paths which appear to mimic the stable manifold of SP4. This suggests that there may in fact be a single trajectory originating form SP2 that connects exactly with SP4. Of course, because the unstable manifold is 2D it is very difficult to numerically find the single curve which makes this connection.

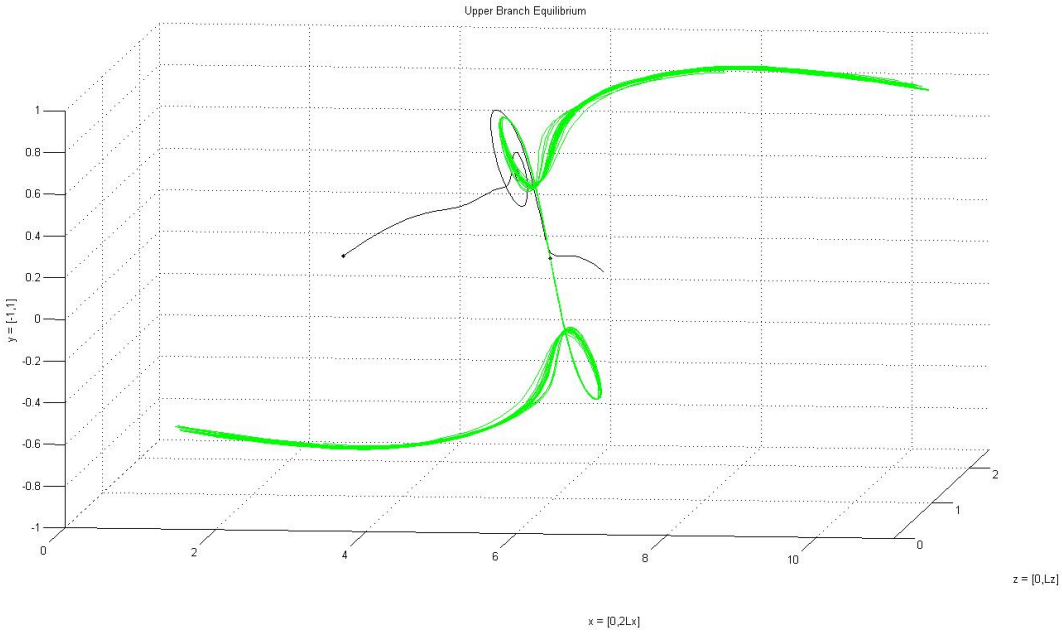

Figure 4.12: Stable manifold of SP2 (black curve) and unstable manifold of SP4 (green surface)

Also, one must question the accuracy of the integration method once these manifolds are evolved far outside of the linear neighborhood.

In the other direction, referring to figure 4.12, we see this time the stable manifold of SP2 (black curve) and the unstable manifold of SP4 (green surface). The black curve appears to "almost" connect with SP4. Again, it could be a numerical issue since close to SP4 the unstable directions will cause rapid stretching of nearby trajectories. However since the green surface is entirely shuffled off in the positive x-direction it looks like something else may be happening.

The loop-de-loop region shared by the stable and unstable manifolds in figure 4.12 suggests the possible existence of another pair of stagnation points (pair because it is symmetric on the lower half). It looks like this point would have a pair of complex eigenvalues with negative real part and a single positive, real eigenvalue. To investigate I have created a more refined grid of velocities which is $144 \times 105 \times 144$. This is three times the $48 \times 35 \times 48$ grid in each dimension and contains about 2.2 million points. At each point $|\mathbf{u}|^2$ is then calculated and at every point that satisfies $|\mathbf{u}|^2 < \epsilon$ for some arbitrarily chosen ϵ, the point is plotted. figure 4.13 shows the result for $\epsilon = 10^{-4}$. The blue blobs are the points which satisfy this condition and they have been plotted along with the same manifolds from figure 4.12. It appears that we have isolated the regions with the already known stagnation points as well as the two regions containing the potential new ones. With a more stringent requirement on ϵ the point in this new

region with smallest value for $|\mathbf{u}|^2$ is found to be (see (4.50) for the precise value)

$$\mathbf{x} \simeq (2.33476, 0.40952, 0.64577)\,, \quad |\mathbf{u}|^2 = 2.75 \times 10^{-6} \tag{4.55}$$

In figure 4.14 this single point (a barely visible red dot) is plotted along with the stable manifold of SP3. This figure looks suggestive not only that this is a stagnation point, but there may also be a heteroclinic connection from this point to SP3.

Clearly the point (4.55) is not the exact stagnation point or $|\mathbf{u}|$ would be 0 to within machine precision. However, the smallest gridpoint value of $|\mathbf{u}|^2$ in the regions where we *know* stagnation points exist is only about 10^{-7}, in the same range. As outlined in sect. 5.1, the next step will be to interpolate recursively until the exact point is found. In addition, no other regions appeared to within these tolerances, so we may have found all of the stagnation points.

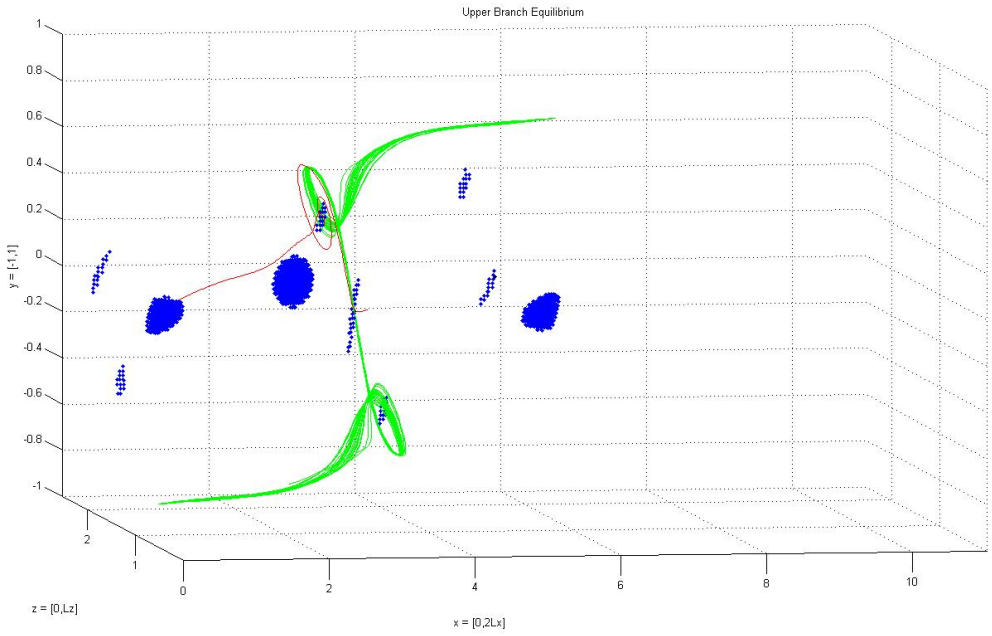

Figure 4.13: Blue points are where velocity squared is very near zero. Shown along with the stable manifold of SP3 and the unstable manifold of SP1.

[**PC May 26, 2008**: moved "local Reynolds number $Re(\mathbf{x})$" musings to sect. 5.4]

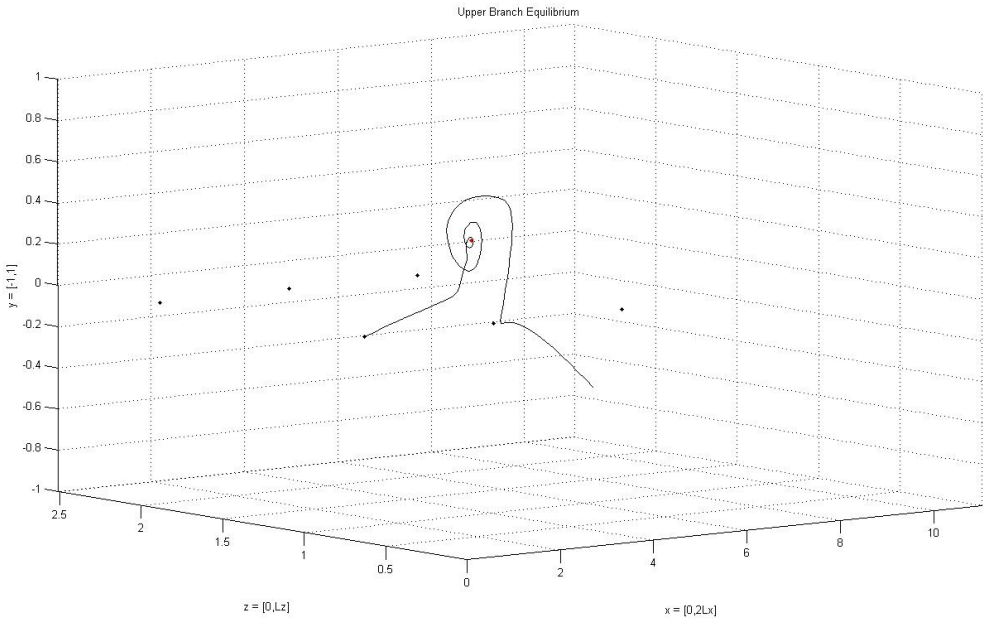

Figure 4.14: Shows a single red point within the tangled region of the stable manifold of SP3. This point has a velocity close to zero and is expected to be very near a stagnation point.

4.8 Matrix of velocity gradients and its eigenvalues

JRE May 15, 2008: For a perturbation $\delta\mathbf{x}$ the change in the velocity field is given by $\delta\mathbf{u} = A\delta\mathbf{x}$ where A is the nine component velocity gradients matrix defined by $A_{ij} = \frac{\partial u_i}{\partial x_j}$. Since $\mathbf{u}$ is given by (7.1), it is a relatively simple extension of this formula to evaluate these partials. To find $\partial\mathbf{u}/\partial y$, one needs to use the relation $\frac{\partial}{\partial y}T_n(y) = nU_{n-1}(y)$ where T_n is the nth Chebyshev polynomial of the first kind and U_n is the nth Chebyshev polynomial of the second kind. Everything else is straightforward.

The eigenvalues of A, evaluated at a stagnation point , give local stability and reveal the qualitative nature of the motions nearby the stagnation point. For the four stagnation points we have so far the eigenvalues, eigenvectors, and velocity gradients matrices are as follows.

$\mathbf{x}_{\rm SP1} = (L_x/2, 0, L_z/4)$: There are 3 real eigenvalues, two positive and one nega-

tive.

$$\lambda^{(1)} = -0.4652099\,, \quad \mathbf{e}^{(1)} = \begin{pmatrix} 0.9844417 \\ 0.1743315 \\ 0.0219779 \end{pmatrix} \tag{4.56}$$

$$\lambda^{(2)} = 0.4008961\,, \quad \mathbf{e}^{(2)} = \begin{pmatrix} 0.5704000 \\ -0.7666749 \\ 0.2947091 \end{pmatrix} \tag{4.57}$$

$$\lambda^{(3)} = 0.0643139\,, \quad \mathbf{e}^{(3)} = \begin{pmatrix} 0.4082166 \\ 0.7525949 \\ 0.5166819 \end{pmatrix} \tag{4.58}$$

The velocity gradients matrix is

$$A = \begin{pmatrix} -0.4305385 & -0.3002042 & 0.8282447 \\ -0.1221356 & 0.2456107 & -0.1675796 \\ 0.0001651 & -0.0828951 & 0.1849278 \end{pmatrix} \tag{4.59}$$

The point is a saddle; It has 1 stable dimension and a 2D plane of instability spanned by $\mathbf{v_2}$ and $\mathbf{v_3}$. The eigenvalues sum to 0, as is required by volume conservation (If you add the values shown here to check this by hand, note that I have rounded them. When they are added on the computer it comes out to be 0 within machine precision, $\sim 10^{-16}$). The stagnation point at $(0, 0, 3L_z/4)$ has the same eigenvalues as this point. It's eigenvectors and velocity gradients matrix differ by a minus sign in the third component (except for A_{33} where the two minuses cancel).

$\mathbf{x}_{\rm SP2} = (L_x/2, 0, 3L_z/4)$: There is one real, negative eigenvalue and a complex pair with positive real part. [8]

$$\lambda^{(1)} = -0.0352362\,, \quad \mathbf{e}^{(1)} = \begin{pmatrix} -0.9452459 \\ -0.1893368 \\ -0.2658228 \end{pmatrix} \tag{4.60}$$

$$\mu^{(2)} \pm i\,\omega^{(2)} = 0.0176181 \pm i\,0.0862176 \tag{4.61}$$

$$\mathbf{e}^{(2)} = \begin{pmatrix} 0.3737950 + 0.0544113i \\ 0.2098940 - 0.4925773i \\ 0.7554000 \end{pmatrix}\,, \quad \mathbf{e}^{(3)} = \begin{pmatrix} 0.3737950 - 0.0544113i \\ 0.2098940 + 0.4925773i \\ 0.7554000 \end{pmatrix}\,.$$

The velocity gradients matrix is

$$A = \begin{pmatrix} -0.0316935 & -0.0708737 & 0.0378835 \\ -0.0250579 & -0.0218884 & 0.0795969 \\ 0.0014742 & -0.1320575 & 0.0535818 \end{pmatrix} \tag{4.62}$$

This stagnation point spirals out in a plane given by the complex pair of eigenvectors. It is stable in one dimension that is dominantly along the x direction. As with

[8] Predrag: rewrite eigenvectors in their real form

the first pair of points, the stagnation point at $(0, 0, L_z/4)$ has the same eigenvalues and again, the velocity gradients matrix is the same except for sign changes in the third component. This follows from the symmetry arguments. We now want to understand the connections between the manifolds.

4.9 Rough sketch of topics

JRE May 12, 2008: After using the sum formula discussed in sect. 7.1 to compute **u** at every point along a trajectory, I have switched to an interpolation method because of run-time issues. Using the previous method, I create an arbitrarily fine set of gridpoint values for **u** and then use a bilinear(trilinear?) interpolation method. (**Note:** To the eye it looks like this works pretty well but I need to look at the numerical values more closely and check the accuracy of the interpolation. How fine should I make the grid? Always need to be careful about approximations in the chaotic regime).

The starting point is clear because we already have four stagnation points predicted from translational symmetries of plane Couette flow. Starting a small sphere of initial conditions around the stagnation points and evolving them forward and backward in time gives a good estimate of the stable and unstable manifolds. Results are shown in figure 4.15. From these we begin to get a feel for the dynamics. Also, I can create movies to show the evolution of a ball of little ink droplets moving through the fluid, but I need to get these from .mat format to mp3's before I can post them anywhere. Being able to visualize the stretching and folding of these material lines and surfaces will be a key point.

This rough visualization of the manifolds is nice, but much better can be done. Since we have a sum formula for computing velocities at any point, by differentiating under the sum it should be a simple matter to compute the $[3 \times 3]$ velocity gradients matrix at any point. Eigenvalues / eigenvectors of this matrix will give linear stability and allow for exact computation of the stable and unstable manifolds. There are several expectations/predictions of what we'll find: (1) Will have one real eigenvalue and one complex pair. Judging from figure 4.15 I'm not sure about this one yet. It certainly looks true for the black/blue stagnation point, but for the other one it seems unclear what is going on. The stretching is strong around this point so it may be that the plane is quickly dominated in one direction and appears to collapse to a line, or it may be that all the eigenvalues are real. (Prepare to edit this section as soon as I have the answer.) (2) The eigenvalues for the two points should be the same but with signs reversed resulting from translational symmetry, and this amounts to time reversal invariance. I'm a little confused on this one, I would appreciate a comment from anyone with an explanation. (3) There is a heteroclinic connection between the stagnation points. Will find out soon, this would be great for using chaos. Apparently the time reversal would force this connection.

After exhausting these four points we will want to find other stagnation points, either by using other symmetries or numerically. The numerical task would involve computing u^2 all along the grid and spotting regions where it is below a given threshold. Then using an interpolation in the small regions the stagnation points can be pinned down. The same eval/evec stable/unstable manifold analysis can then be done for any

other stagnation point.

The long term goal after all of this is of course to compute mixing and diffusion properties; Lyapunov exponents, material stretching, striation thickness, time to mix etc... Most investigations like this tend to be in two dimensional closed systems, but if we find we have good Lagrangian chaos, there is no reason not to do it here.

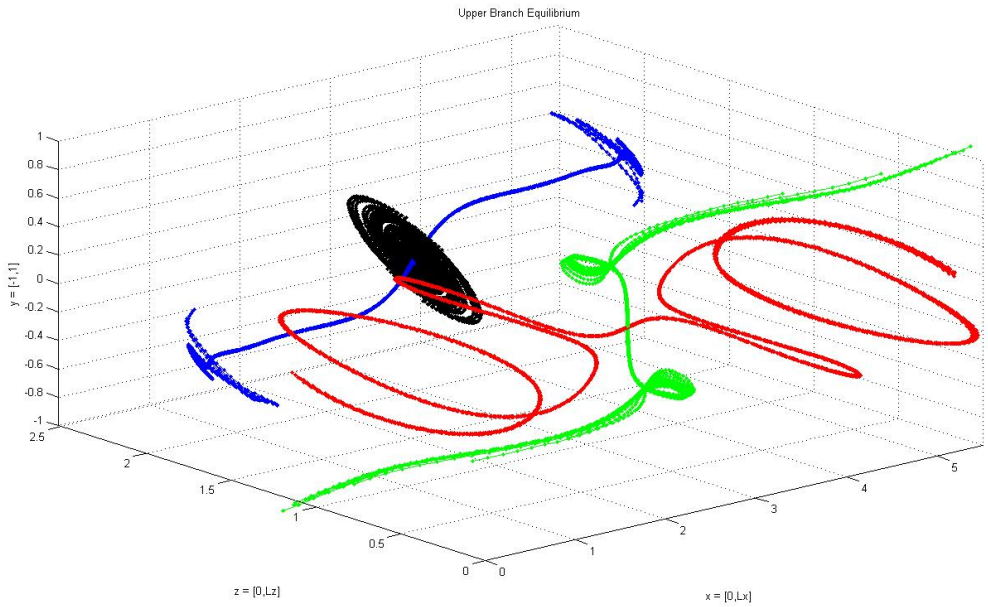

Figure 4.15: Stable and unstable manifolds of the stagnation points $\mathbf{x}_{\rm SP1} = (L_x/2, 0, L_z/4)$ and $\mathbf{x}_{\rm SP2} = (L_x/2, 0, 3L_z/4)$. Black and green are unstable.

4.10 Notes on mixing

General discussion and notes about mixing in fluids, largely taken from the book by J.M. Ottino (see reading assignments).

Coming soon.

4.11 Mixing and stagnation points for EQ2

JRE April 29, 2008: Our starting point is the data set computed by Gibson [88] of the Nagata/Walleffe "upper branch" equilibrium EQ2, for $Re = 400$, the Waleffe [89] small-aspect cell

$$\Omega_{\rm w03} = [L_x, 2, L_z] = [2\pi/1.14, 2, 4\pi/5] = [5.511566, 2, 2.513274]\,. \qquad (4.63)$$

To begin looking at the evolution of Lagrangian tracers in the equilibrium EQ2, I have first integrated a grid of initial points. The grid is chosen to lie in the $[y, z]$ plane, centered at $x = L_x/2$. The initial points are equally spaced, and offset by one position from the edge of the box. If the number of points is chosen to be one less than a multiple of 4, there will be points starting at $\mathbf{x}_{\rm SP1} = (L_x/2, 0, L_z/4)$ and $\mathbf{x}_{\rm SP2} = (L_x/2, 0, 3L_z/4)$. Similarly, if we make the grid be centered at x = 0, we will have points starting at $(0, 0, L_z/4)$ and $(0, 0, 3L_z/4)$. The trajectories are run for 15 seconds, and the results of this are shown in figure 4.16 (a) and figure 4.17 (a). [9]

Invariance under the symmetry group $\mathbf{S}$, explained by JH in sect. 4.12, implies the existence of 4 stagnation points (4.73). In figure 4.16(b) and figure 4.17(b) the figures from part (a) have been rotated to almost a y-z projection in order to reveal these stagnation points. The behavior of trajectories near these fixed points seems to reveal "what kind" of fixed points they are. The point at $3L_z/4$ in figure 4.16(b) appears to be an unstable out-spiral, whereas the point at $L_z/4$ is probably hyperbolic. There is also some other interesting behavior going on near the point at $L_z/4$. The next step is probably to look at eigenvalues and stable/unstable manifold of these stagnation points.

JFG April 30, 2008 The plots of tracers and the derivation of stagnation points from symmetries are very interesting.

I see from figure 4.17 and figure 4.16 that you're plotting tracers for the difference from laminar flow. (You can see $u \to 0$ as $y \to \pm 1$.) I don't know if this is intentional. If it's not, sorry, we haven't been sufficiently clear on the definitions of data we gave you. We usually work with $\mathbf{u}$ defined as the difference from laminar flow, so that the total velocity field $\mathbf{u}_{\rm tot} = \mathbf{u} + y\hat{\mathbf{x}}$. So you might want to add the laminar flow $y\hat{\mathbf{x}}$ on to $\mathbf{u}$ before computing tracers. That'll produce $u \to \pm 1$ as $y \to \pm 1$. The stagnation points are all at $y = 0$, so they will not change.

JRE May 02, 2008 No, that was not intentional. I had forgotten that the velocity fields were computed *from* laminar. From now on all plots are of $\mathbf{u}_{\rm tot}$.

4.12 Symmetry and stagnation points

Plane Couette flow is invariant under two reflections σ_1, σ_2 and a continuous two-parameter group of translations $\tau(d_x, d_z)$:

$$\begin{aligned} \sigma_1\,[u, v, w](x, y, z) &= [u, v, -w](x, y, -z) \\ \sigma_2\,[u, v, w](x, y, z) &= [-u, -v, w](-x, -y, z) \\ \tau(d_x, d_z)[u, v, w](x, y, z) &= [u, v, w](x + d_x, y, z + d_z)\,. \end{aligned} \tag{4.64}$$

The Navier-Stokes equations and boundary conditions are invariant for any symmetry s in the group generated by these elements: $\partial(s\mathbf{u})/\partial t = s(\partial\mathbf{u}/\partial t)$.

The plane Couette symmetries can be interpreted geometrically in the space of fluid velocity fields. Let $\mathbb{U}$ be the space of square-integrable, real-valued velocity fields that

[9] JRE: The figures need some editing. It's almost impossible to read the axis labels. Also, they won't go where I want them to!

satisfy the kinematic conditions of plane Couette flow:

$$\mathbb{U} = \{\mathbf{u} \in L^2(\Omega) \mid \nabla \cdot \mathbf{u} = 0,\ \mathbf{u}(x, \pm 1, z) = 0,\\ \mathbf{u}(x, y, z) = \mathbf{u}(x + L_x, y, z) = \mathbf{u}(x, y, z + L_z)\}\,. \tag{4.65}$$

[10] The continuous symmetry $\tau(d_x, d_z)$ maps each state $\mathbf{u} \in \mathbb{U}$ to a $2d$ torus of states with identical dynamic behavior. This torus in turn is mapped to four equivalent tori by the subgroup $\{1, \sigma_1, \sigma_2, \sigma_1\sigma_2\}$. In general a given state in $\mathbb{U}$ has four $2d$ tori of dynamically equivalent states.

Most of the Eulerian equilibria that we know of so far are invariant under the 'shift-reflect' symmetry $s_1 = \tau(L_x/2, 0)\,\sigma_1$ and the 'shift-rotate' symmetry $s_2 = \tau(L_x/2, L_z/2)\,\sigma_2$. These symmetries form a subgroup $S = \{1, s_1, s_2, s_3\}$, $s_3 = s_1 s_2$, which is isomorphic to the Abelian dihedral group D_2. The group acts on velocity fields as:

$$\begin{aligned} s_1\,[u, v, w](x, y, z) &= [u, v, -w](x + L_x/2,\ y,\ -z)\\ s_2\,[u, v, w](x, y, z) &= [-u, -v, w](-x + L_x/2,\ -y,\ z + L_z/2)\\ s_3\,[u, v, w](x, y, z) &= [-u, -v, -w](-x,\ -y,\ -z + L_z/2)\,. \end{aligned} \tag{4.66}$$

Consider next the subgroup $S_3 = \{1, s_3\} \subset S$ (isomorphic to dihedral group D_1). The s_3 operation flips both the streamwise x and the spanwise z, thus eliminating invariance under both x and z continuous translations. [11]

Let $\mathbb{U}$ be the space of square-integrable, real-valued velocity fields that satisfy the kinematic conditions of plane Couette flow:

$$\mathbb{U} = \{\mathbf{u} \in L^2(\Omega) \mid \nabla \cdot \mathbf{u} = 0,\ \mathbf{u}(x, \pm 1, z) = 0,\\ \mathbf{u}(x, y, z) = \mathbf{u}(x + L_x, y, z) = \mathbf{u}(x, y, z + L_z)\}\,. \tag{4.67}$$

We denote the S-invariant subspace of states invariant under symmetries (4.66) by

$$\mathbb{U}_c = \{\mathbf{u} \in \mathbb{U} \mid s_j\mathbf{u} = \mathbf{u}\,,\ \ s_j \in S\}\,, \tag{4.68}$$

and the S_3-invariant subspace by

$$\mathbb{U}_{s3} = \{\mathbf{u} \in \mathbb{U} \mid s_3\mathbf{u} = \mathbf{u}\,,\ \ s_1\mathbf{u} \neq \mathbf{u}\,,\ \ s_2\mathbf{u} \neq \mathbf{u}\}\,, \tag{4.69}$$

where $\mathbb{U}_c \subset \mathbb{U}_{s3} \subset \mathbb{U}$. $\mathbb{U}_c$ and $\mathbb{U}_{s3}$ are flow-invariant subspaces: states initiated in either remain within it under the Navier-Stokes dynamics.

Idempotency of s_3 leads to projection operators

$$\mathbf{P}_+ = \frac{1}{2}(\mathbf{1} + s_3)\,, \qquad \mathbf{P}_- = \frac{1}{2}(\mathbf{1} - s_3)\,. \tag{4.70}$$

[10] JRE: Shouldn't we say $\mathbf{u} = \pm 1$ at the walls for consistency?

[11] Predrag: do we need this in this paper?:
"$s_3\mathbf{u} = \mathbf{u}$ implies $[u, v, w](x, y, z) = [-u, -v, -w](-x, -y, -z + L_z/2)$, which requires $\mathbf{u} = 0$ at four points $(x, y, z) = (0, 0, L_z/4); (0, 0, 3L_z/4); (L_x/2, 0, L_z/4); (L_x/2, 0, 3L_z/4)$. "

Translations of half the cell length in the spanwise and/or streamwise directions commute with S. These operators generate a discrete subgroup of the continuous translational symmetry group $SO(2) \times SO(2)$:

$$T = \{e, \tau_x, \tau_z, \tau_{xz}\}\,, \qquad \tau_x = \tau(L_x/2, 0)\,,\ \tau_z = \tau(0, L_z/2)\,,\ \tau_{xz} = \tau_x \tau_z\,. \quad (4.71)$$

Since the action of T commutes with that of S, the three half-cell translations $\tau_x \mathbf{u}$, $\tau_z \mathbf{u}$, and $\tau_{xz} \mathbf{u}$ of $\mathbf{u} \in \mathbb{U}_c$ are also in $\mathbb{U}_c$. Similarly, τ_{xz} commutes with S_3, so S_3-invariant solutions appear in eight copies. [12]

JH April 28, 2008: From the form of s_3, we can see that any Eulerian *equilibrium* that is invariant under has 4 Lagrangian stagnation points which satisfy the condition:

$$(x, y, z) = (-x, -y, -z + L_z/2) \quad (4.72)$$

There are 4 points which satisfy this constraint:

$$\begin{aligned} \mathbf{x}_{\text{SP1}} &= (L_x/2, 0, L_z/4) \\ \mathbf{x}_{\text{SP2}} &= (L_x/2, 0, 3L_z/4) \\ \mathbf{x}_{\text{SP3}} &= (0, 0, L_z/4) \\ \mathbf{x}_{\text{SP4}} &= (0, 0, 3L_z/4)\,. \end{aligned} \quad (4.73)$$

Due to the periodic boundary conditions $(L_x, 0, L_z/4)$ = SP3 and $(L_x, 0, 3L_z/4)$ = SP4. Also of note is the fact that there can exist no s_3-invariant relative equilibria, since s_3 operation flips both the x and z axes.

PC May 25, 2008: moved sect. 7.1 to chapter 7.

4.13 Notational conventions

Predrag, May 12, 2008: In Lagrangian mixing we need to distinguish between $3D$ physical fluid flow (for a given invariant solution) and the dynamical ∞-dimensional state space flow.

We distinguish the two by using physically motivated nomenclature for $3D$ physical fluid flow: We shall refer to the $3D$ point $\mathbf{x}$ for which $\mathbf{u}(\mathbf{x}_{\text{eq}}) = 0$ as the *stagnation point* $\mathbf{x}_{\text{eq}}$, and the moving point $\mathbf{x}$(t) for which $\mathbf{u}(\mathbf{x}_{\text{tw}}(t)) = 0$, $\mathbf{x}_{\text{tw}}(t) - \mathbf{c}t = \mathbf{x}_{\text{tw}}(0)$ as the *traveling stagnation point* $\mathbf{x}_{\text{tw}}$(t).

(to be continued: velocity gradients matrix, etc..)

Predrag to Jonathan, Oct 13, 2007: Relative equilibria are not periodic, they are stationary in the velocity $\mathbf{c}$ co-moving frame. Rather than using "period of T" description (such as "x traveling with a period of $T = 169.62747092815$"), state that $TW_{\pm 1}$ has velocity $c_x = L_x/T$?

[12] Predrag: incorporate halcrow blog JFG comment for the the S_3-invariant claim, please: if you agree, comment out this footnote.

4.14 Integrating velocity fields

Predrag Nov 2, 2007 to Kai Schneider:
John Elton is planning to use some of the exact plane Couette flow solutions computed by Waleffe, Viswanath, Gibson and Halcrow (data sets are on channelfow.org) and study Lagrangian tracer trajectories for such solutions. Marie Farge (farge@lmd.ens.fr) tells me that many people do this inaccurately, but you know how to do it right. Let us know what we should read not to waste time on not doing it right?
Kai Schneider: (kschneid@cmi.univ-mrs.fr)
Concerning Lagrangian particles: it is important to use the right techniques for time integration and for interpolation of the velocity (and acceleration) for computing them accurately.

For time integration we are using a second order Runge-Kutta scheme and for space interpolation a bicubic (in 2d) scheme.

There is a nice recent paper by Homann, Dreher and Grauer [79] and an older one by P.K. Yeung and Pope [80] (you have the specialist on that just next 10 buildings away).

4.15 Passive scalar advection?

PC Nov 2, 2007: The other thing we might try is passive scalar transport using these velocity fields (but that I really have barely started thinking about).

Very sketchy:

Given a velocity field, densities (passive scalars?) are advected by th *Fokker-Planck equation*

$$\partial_t \rho + \partial_i(\rho v_i) = D\,\partial^2 \rho. \tag{4.74}$$

The left hand side, $d\rho/dt = \partial_t\rho + \partial\cdot(\rho v)$, is deterministic, with the continuity equation recovered in the weak noise limit $D \to 0$. The right hand side describes the diffusive transport in or out of the material particle volume. If the density is lower than in the immediate neighborhood, the local curvature is positive, $\partial^2\rho > 0$, and the density grows. Conversely, for negative curvature diffusion lowers the local density, thus smoothing the variability of ρ.

Not sure that this is the thing we want to investigate, and sure do not know how to think about the diffusive part $D\,\partial^2\rho$. Easier to try playing with tracer particles first...
JFG 2008-04-29: If we want to do this, it would not be hard to integrate the Fokker-Planck equation using channelflow, at least with an explicit time-stepping method. Express the probability density as a 1d FlowField, compute the $\partial_i(\rho v_i)$ and $D\,\partial^2\rho$ terms using differential operators, and add them together using Adams-Bashforth, Runge-Kutta, or similar formulae to get an update equation for the density. It would not take many lines of code.

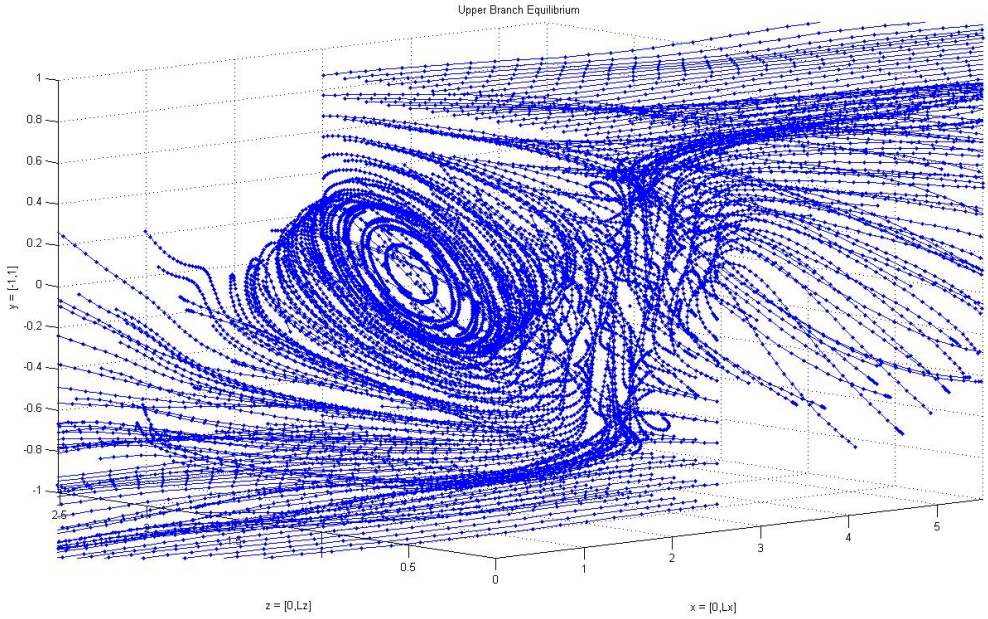

(a)

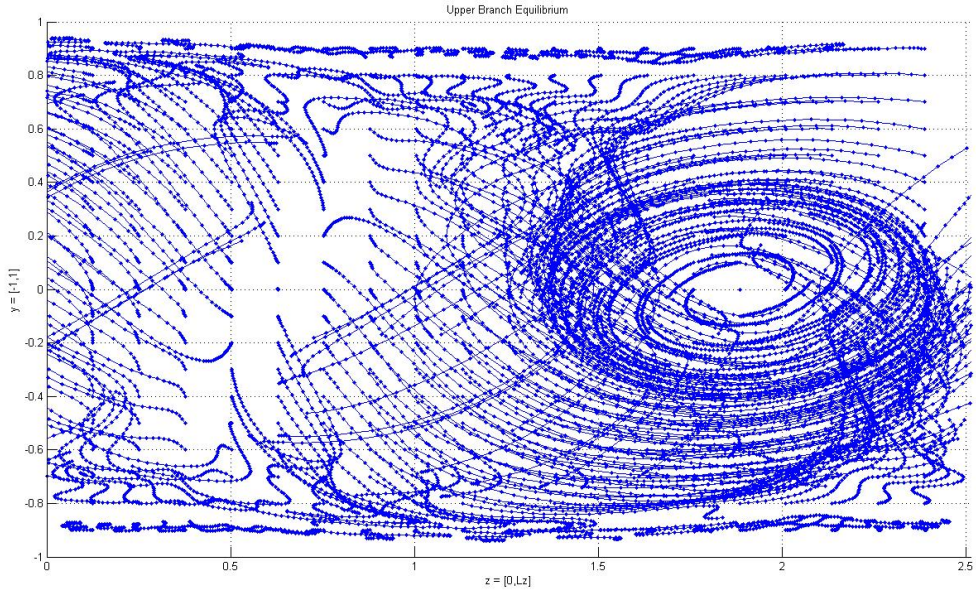

(b)

Figure 4.16: (a) Grid of 19×19 initial points in the $[y, z]$ plane, centered at $x = L_x/2$; integrated for 15 time units. (b) Rotated to show the 2 stagnation points.

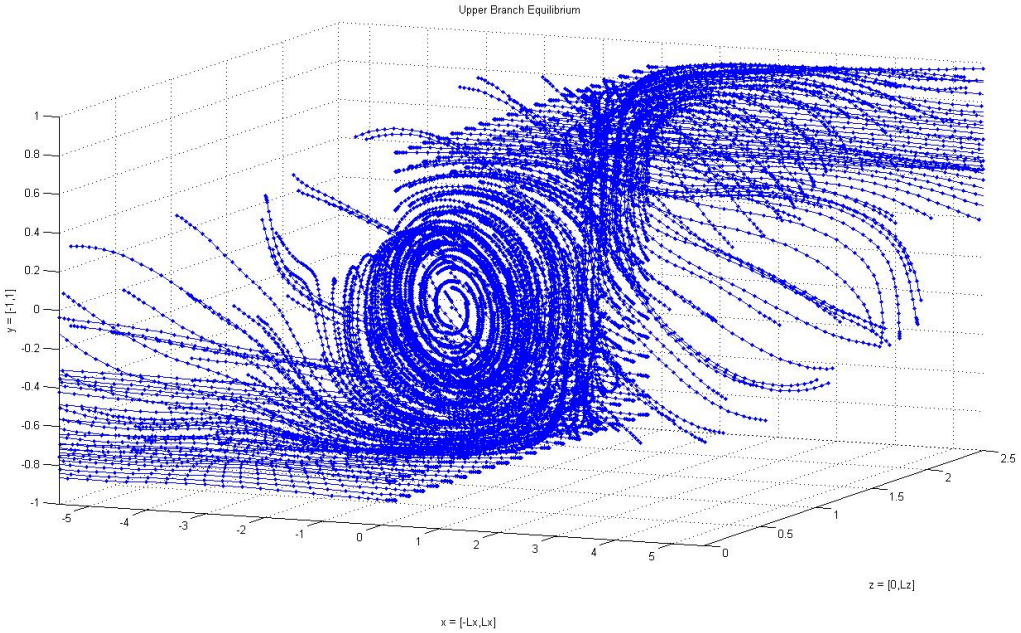

(a)

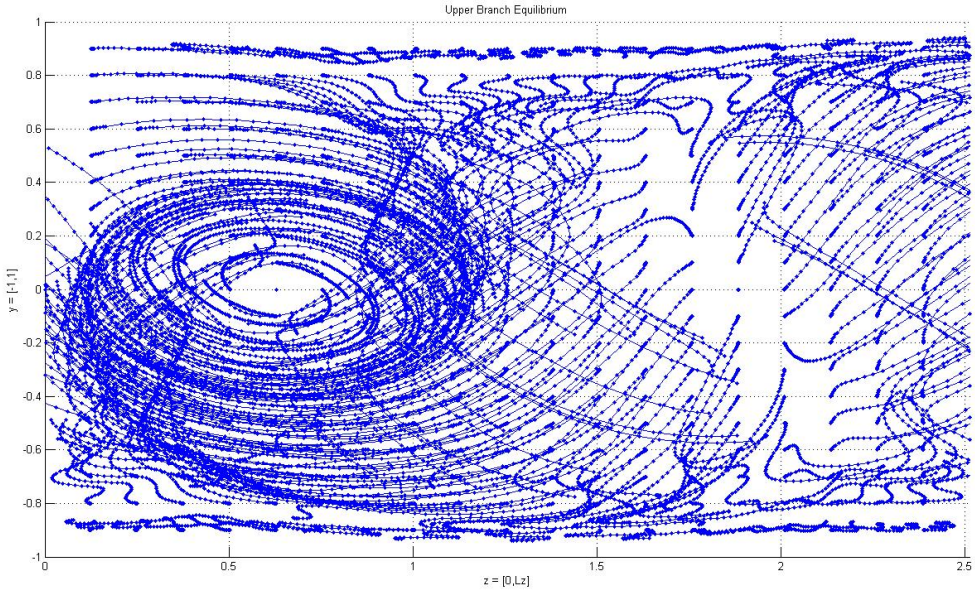

(b)

Figure 4.17: (a) Grid of 19×19 initial points in the $[y, z]$ plane, centered at $x = 0$; integrated for 15 time units. (b) Rotated to show the other 2 stagnation points.

Chapter 7

Channelflow

[1]

7.1 Lagrangian streamlines

JRE April 25, 2008: In order to integrate streamlines of plane Couette flow and follow the paths of tracer particles, it is first necessary to have a numerically accurate equilibrium $3D$-velocity field.

The starting point for this task is to obtain the previously computed FlowField data for a given equilibrium, e.g. upper branch, lower branch, etc... These are made available at the website `Channelflow.org` as is most of the information I am about to summarize about FlowFields. Essentially, the FlowField data contains a long array of numbers which are the spectral coefficients of the expansion of a velocity field $\mathbf{u}(\mathbf{x})$. The form of the expansion is

$$\mathbf{u}(\mathbf{x}) = \sum_{m_y=0}^{M_y-1} \sum_{m_x=0}^{M_x-1} \sum_{m_z=0}^{M_z-1} \hat{\mathbf{u}}_{m_x,m_y,m_z} \bar{T}_{m_y}(y) e^{2\pi i(k_x x/L_x + k_z z/L_z)} + \text{(c.c.)} \qquad (7.1)$$

The $\hat{\mathbf{u}}$'s are the spectral coefficients - the information stored in a FlowField. The $\bar{T}(y)$'s are Chebyshev polynomials defined on the interval [a,b] (in most cases [-1,1]). The order of the summations, although mathematically irrelevant, reflects the order in which the spectral coefficients are stored as a data array. z is the innermost loop, then x, then y, and finally the vector component of $\mathbf{u}(\mathbf{x})$ is the outermost loop. For a given FlowField the upper bounds on the sums are known from the geometry, and the k's are related to the m's through the following relations:

$$k_x = \begin{cases} m_x & 0 \le m_x \le M_x/2 \\ m_x - M_x & M_x < m_x < M_x \end{cases} \qquad (7.2)$$

$$k_z = m_z \qquad 0 \le m_z < M_z\,. \qquad (7.3)$$

[1] `elton/blog/channelflow.tex`, rev. 176: last edit by Predrag Cvitanović, 12/29/2013

Hence, with a knowledge of the spectral coefficients we can compute $\mathbf{u}(\mathbf{x})$ by evaluating this sum at a particular $\mathbf{x} = (x, y, z)$.

Various internal functions within `Channelflow.org` have been written to compute $\mathbf{u}$ on a set of gridpoints. It is possible, by interpolation of the velocity fields on these gridpoint values, to integrate a trajectory with great computational speed. However this will not be nearly as accurate as evaluating the sum (7.1), and currently we don't really know whether the first method would give a reasonable approximation at all. For this reason the current strategy is to evaluate (7.1) to give the exact velocity field at every point along a trajectory. Summing over 10^5 coefficients at every step sounds slow and inefficient, and it surely is compared to the interpolation method. But luckily it doesn't seem to be *too* slow. I have written a function in Matlab that performs this computation for a single point in about 0.01 seconds. It is certainly possible that this could be made faster. The code has been checked to be correct by picking an (x, y, z) coordinate that *happens* to lie on a gridpoint value and then comparing the result to the value given by the internal `Channelflow.org` functions. If, for example, we wanted to compute trajectories for 50 initial points for 500 time steps each this would still only take less than 5 minutes (ignoring the time needed to perform a Runge-Kutta step, or whatever).

7.1.1 Specifics

The new `Channelflow.org` function "field2ascii-spectral.cpp" converts the spectral coefficients to ascii format, which is readable by Matlab. The command
./field2ascii-spectral.x u u-whatev
takes in the FlowField u.ff and produces the files u-whatev.asc and u-whatev-geom.asc. In Matlab, the commands load('u-whatev.asc') and load('u-whatev-geom.asc') create vectors containing all of the necessary data. The newly written Matlab script "trajectory.m" takes this information and performs the sum (7.1). (Note that all of the hyphens in these file names should actually be underscores, I just don't know how to display underscores in LaTEX). So I am now basically ready to start playing with tracers.

7.1.2 OpenMP-parallelize channelflow

7.1.3 Benchmark channelflow against similar codes

7.1.4 Get channelflow running on cluster (as is)

Aug 2007: DONE now runs on PACE cluster

Bibliography

[1] L. Sirovich. Turbulence and the dynamics of coherent structures. Part II: Symmetries and transformations. *Q. Appl. Math.*, 45(3):573–582, 1987.

[2] S. Froehlich and P. Cvitanović. Reduction of continuous symmetries of chaotic flows by the method of slices. *Commun. Nonlinear Sci. Numer. Simul.*, 17:2074–2084, 2012. arXiv:1101.3037.

[3] J. F. Gibson, J. Halcrow, and P. Cvitanović. Visualizing the geometry of state-space in plane Couette flow. *J Fluid Mech.*, 611:107–130, 2008. arXiv:0705.3957.

[4] M. Budišić and I. Mezić. Geometry of the ergodic quotient reveals coherent structures in flows. *Physica D*, 241:1255–1269, 2012. arXiv:1204.2050.

[5] G. Mathew, I. MeziĆ, S. Grivopoulos, U. Vaidya, and L. Petzold. Optimal control of mixing in Stokes fluid flows. *J. Fluid Mech.*, 580:261–281, 2007.

[6] C. Foias, O. Manley, R. Rosa, and R. Temam. *Navier–Stokes Equations and Turbulence*. Cambridge Univ. Press, Cambridge, 2001.

[7] R. A. Adams and J. J. F. Fournier. *Sobolev spaces*. Academic press, New York, 2003.

[8] L. D. Landau. On the problem of turbulence. *Akad. Nauk. Doklady*, 44:339, 1944.

[9] E. Hopf. A mathematical example displaying features of turbulence. *Comm. Appl. Math.*, 1:303–322, 1948.

[10] F. Christiansen, P. Cvitanović, and V. Putkaradze. Spatio-temporal chaos in terms of unstable recurrent patterns. *Nonlinearity*, 10:55–70, 1997.

[11] P. Holmes, J. L. Lumley, G. Berkooz, and C. W. Rowley. *Turbulence, Coherent Structures, Dynamical Systems and Symmetry*. Cambridge Univ. Press, Cambridge, second edition, 2012.

[12] E. Hopf. Abzweigung einer periodischen lösung. *Bereich. Sächs. Acad. Wiss. Leipzig, Math. Phys. Kl*, 94:19, 1942.

[13] H. Kielhöfer. Hopf bifurcation at multiple eigenvalues. *Arch. Ration. Mech. Anal.*, 69:53–83, 1979.

[14] D. W. Moore and E. A. Spiegel. A thermally excited nonlinear oscillator. *Astrophys. J.*, 143:871, 1966.

[15] M. Nagata. Three-dimensional finite-amplitude solutions in plane Couette flow: bifurcation from infinity. *J. Fluid Mech.*, 217:519–527, 1990.

[16] M. Nagata. Three-dimensional traveling-wave solutions in plane Couette flow. *Phys. Rev. E*, 55:2023–2025, 1997.

[17] D. Viswanath. Recurrent motions within plane Couette turbulence. *J. Fluid Mech.*, 580:339–358, 6 2007.

[18] G. Kawahara, S. Kida, and L. Van Veen. Unstable periodic motion in turbulent flows. *Nonlin. Proc. Geophys.*, 13(5):499–507, 2006.

[19] D. Auerbach, P. Cvitanović, J.-P. Eckmann, G. Gunaratne, and I. Procaccia. Exploring chaotic motion through periodic orbits. *Phys. Rev. Lett.*, 58:23, 1987.

[20] J.-P. Eckmann, S. O. Kamphorst, and D. Ruelle. Recurrence plots of dynamical systems. *Europhys. Lett.*, 4:973, 1987.

[21] P. Cvitanović and J. F. Gibson. Geometry of turbulence in wall-bounded shear flows: Periodic orbits. *Phys. Scr. T*, 142:014007, 2010.

[22] D. Viswanath. Recurrent motions within plane Couette turbulence. unpublished, arXiv:physics/0604062, 2006.

[23] P. Cvitanović and Y. Lan. Turbulent fields and their recurrences. In N. Antoniou, editor, *Proceedings of 10th International Workshop on Multiparticle Production: Correlations and Fluctuations in QCD*, Singapore, 2003. World Scientific. arXiv:nlin.CD/0308006.

[24] Y. Lan and P. Cvitanović. Variational method for finding periodic orbits in a general flow. *Phys. Rev. E*, 69:016217, 2004. arXiv:nlin.CD/0308008.

[25] J. Yang and T. I. Lakoba. Universally-convergent squared-operator iteration methods for solitary waves in general nonlinear wave equations. *Studies in Applied Mathematics*, 118(2):153–197, 2007.

[26] J. Hopcroft and R. Kannan. Foundations of data science. In preparation, 2014.

[27] E. J. Wegman and J. L. Solka. On some mathematics for visualizing high dimensional data. *Sankhyā: Indian J. Statistics, Ser. A*, pages 429–452, 2002.

[28] Y. Lan, C. Chandre, and P. Cvitanović. Variational method for locating invariant tori. *Phys. Rev. E*, 74:046206, 2006. arXiv:nlin.CD/0508026.

[29] Y. Lan. *Dynamical systems approach to 1-d spatiotemporal chaos - A cyclist's view*. PhD thesis, Georgia Inst. of Technology, 2004. ChaosBook.org/projects/theses.html.

[30] X. Ding and P. Cvitanović. Periodic eigendecomposition and its application in Kuramoto-Sivashinsky system. arXiv:1406.4885, 2014.

[31] E. Siminos and P. Cvitanović. Continuous symmetry reduction and return maps for high-dimensional flows. *Physica D*, 240:187–198, 2011.

[32] P. Cvitanović, R. Artuso, R. Mainieri, G. Tanner, and G. Vattay. *Chaos: Classical and Quantum*. Niels Bohr Institute, Copenhagen, 2014. ChaosBook.org.

[33] O. Biham and W. Wenzel. Characterization of unstable periodic orbits in chaotic attractors and repellers. *Phys. Rev. Lett.*, 63:819, 1989.

[34] W. R. Smith and J. G. Wissink. Asymptotic analysis of the attractors in two-dimensional kolmogorov flow, 2017. Eur. J. Appl. Math., to appear.

[35] N. Platt, L. Sirovich, and N. Fitzmaurice. An investigation of chaotic Kolmogorov flows. *Phys. Fluids A*, 3:681–696, 1991.

[36] J. S. A. Green. Two-dimensional turbulence near the viscous limit. *J. Fluid M.*, 62:273–287, 1974.

[37] L. R. Keefe. Dynamics of perturbed wavetrain solutions to the Ginzburg-Landau equation. *Stud. Appl. Math.*, 73:91–153, 1985.

[38] G. Birkhoff and S. MacLane. *A brief survey of modern algebra*. Macmillan, 1963.

[39] J. Killingbeck. Group theory and topology in solid state physics. *Rep. Prog. Phys.*, 33:533, 1970.

[40] V. I. Arnold. Kolmogorov's hydrodynamic attractors. *Proc. R. Soc. Lond. A*, 434(1890):19–22, 1991.

[41] G. J. Chandler and R. R. Kerswell. Invariant recurrent solutions embedded in a turbulent two-dimensional Kolmogorov flow. *J. Fluid M.*, 722:554–595, 2013. arXiv:1207.4682.

[42] D. Lucas and R. R. Kerswell. Spatiotemporal dynamics in 2D Kolmogorov flow over large domains. *J. Fluid Mech.*, 750:518–554, 2014. arXiv:1308.3356.

[43] D. Lucas and R. R. Kerswell. Recurrent flow analysis in spatiotemporally chaotic 2-dimensional Kolmogorov flow. *Phys. Fluids*, 27:518–554, 2015.

[44] R. Mitchell Jr. *Transition to turbulence and mixing in a quasi-two-dimensional Lorentz force-driven Kolmogorov flow*. PhD thesis, School of Physics, Georgia Inst. of Technology, Atlanta, 2013. ChaosBook.org/projects/theses.html.

[45] C. Huygens. *L'Horloge à pendule*. Swets & Zeitlinger, Amsterdam, 1673, 1967.

[46] H. Poincaré. Sur les solutions périodiques et le principe de moindre action. *C. R. Acad. Sci. Paris*, 123:915–918, 1896.

[47] U. Frisch. *Turbulence*. Cambridge Univ. Press, Cambridge, UK, 1996.

[48] R. Hoyle. *Pattern Formation: An Introduction to Methods*. Cambridge Univ. Press, Cambridge, 2006.

[49] J. E. Marsden and T. S. Ratiu. *Introduction to Mechanics and Symmetry*. Springer, New York, 1999.

[50] M. Golubitsky and I. Stewart. *The symmetry perspective*. Birkhäuser, Boston, 2002.

[51] R. Gilmore and C. Letellier. *The Symmetry of Chaos*. Oxford Univ. Press, Oxford, 2007.

[52] W. G. Harter. *Principles of Symmetry, Dynamics, and Spectroscopy*. Wiley, New York, 1993.

[53] J. Halcrow. *Geometry of turbulence: An exploration of the state-space of plane Couette flow*. PhD thesis, School of Physics, Georgia Inst. of Technology, Atlanta, 2008. `ChaosBook.org/projects/theses.html`.

[54] N. Andersson and G. L. Comer. Relativistic fluid dynamics: Physics for many different scales. *Living Reviews in Relativity*, 10, 2007.

[55] B. F. Schutz. *Geometrical Methods of Mathematical Physics*. Cambridge Univ. Press, Cambridge, 1980.

[56] B. Carter and N. Chamel. Covariant analysis of Newtonian multi-fluid models for neutron stars I: Milne-Cartan structure and variational formulation. *Int. J. Mod. Phys. D*, 13:291–325, 2004. `arXiv:astro-ph/0305186`.

[57] J. A. Schouten. *Tensor Analysis for Physicists*. Dover, New York, 1989.

[58] M. C. Spruill. Asymptotic distribution of coordinates on high dimensional spheres. *Elect. Comm. in Probab.*, 12:234–247, 2007.

[59] J. Frøyland. Lyapunov exponents for multidimensional orbits. *Phys. Lett. A*, 97:8 – 10, 1983.

[60] J. Frøyland. Some symmetric, two-dimensional, dissipative maps. *Physica D*, 8:423–434, 1983.

[61] J. Frøyland and K. H. Alfsen. Lyapunov exponent spectra for the Lorenz model. *Phys. Rev. A*, 29:2928–2931, 1984.

[62] K. H. Alfsen and J. Frøyland. Systematics of the Lorenz model at $\sigma = 10$. *Phys. Scr.*, 31:15, 1985.

[63] P. Mullen, A. McKenzie, D. Pavlov, L. Durant, Y. Tong, E. Kanso, J. E. Marsden, and M. Desbrun. Discrete Lie advection of differential forms. *Foundations of Comp. Math.*, 11:131–149, 2011.

[64] P. Cvitanović and G. Vattay. Entire Fredholm determinants for evaluation of semi-classical and thermodynamical spectra. *Phys. Rev. Lett.*, 71:4138–4141, 1993. arXiv:chao-dyn/9307012.

[65] N. B. Budanur, D. Borrero-Echeverry, and P. Cvitanović. Periodic orbit analysis of a system with continuous symmetry - a tutorial. *Chaos*, 25:073112, 2015. arXiv:1411.3303.

[66] J. Cresson, A. Daniilidis, and M. Shiota. On the first integral conjecture of René Thom. *B. Sci. Math.*, 132(7):625 – 631, 2008.

[67] E. Gouillart, O. Dauchot, J.-L. Thiffeault, and S. Roux. Open-flow mixing: Experimental evidence for strange eigenmodes. *Phys. Fluids*, 21:023603, 2009. arXiv:0807.1723.

[68] J.M. Ottino. *The Kinematics of Mixing: Stretching, Chaos and Transport*. Cambridge Univ. Press, Cambridge, 1989.

[69] H. Chaté, E. Villermaux, and J.-M. Chomaz. *Mixing - chaos and turbulence*. Kluwer, New York, 1999.

[70] T. H. Solomon, B. R. Wallace, . S. Miller, and C. J. L. Spohn. Lagrangian chaos and multiphase processes in vortex flows. *Comm. Nonlinear Sci. Numer. Simul.*, 8:239–252, 2003.

[71] M. A. Fogleman, M. J. Fawcett, and T. H. Solomon. Lagrangian chaos and correlated Levy flights in a non-Beltrami flow: Transient versus long-term transport. *Phys. Rev. E*, 63:020101, 2001.

[72] Y. Du and E. Ott. Growth rates for fast kinematic dynamo instabilities of chaotic fluid flows. *J. Fluid Mech.*, 257:265–288, 2006.

[73] C. Castelain, A. Mokrani, Y. Le Guer, and H. Peerhossaini. Experimental study of chaotic advection regime in a twisted duct flow. *European J. Mechanics B*, 20:205–232, 2001.

[74] F. d'Ovidio, J. Isern-Fontanet, C. Lopez, E. Hernandez-Garcia, and E. Garcia-Ladona. Comparison between Eulerian diagnostics and finite-size lyapunov exponents computed from altimetry in the Algerian basin. arXiv:0807.3848, 2008.

[75] G. Károly and T. Tél. Chaotic tracer scattering and fractal basin boundaries in a blinking vortex-sink system. *Phys. Reports*, 290:125–147, 1997.

[76] T. Tél, G. Károlyi, Á. Péntek, I. Scheuring, Z. Toroczkai, C. Grebogi, and J. Kadtke. Chaotic advection, diffusion, and reactions in open flows. *CHAOS*, 10:89–98, 2000.

[77] H. R. Dullin and J. D. Meiss. Quadratic volume-preserving maps: Invariant circles and bifurcations, 2008. arXiv:0807.0678.

[78] M. S. Chong, A. E. Perry, and B. J. Cantwell. A general classification of three-dimensional flow fields. *Phys. Fluids*, 2:765–777, 1990.

[79] H. Homann, J. Dreher, and R. Grauer. Impact of the floating-point precision and interpolation scheme on the results of DNS of turbulence by pseudo-spectral codes. *Comp. Phys. Comm.*, 177:560–565, 2007. arXiv:0705.3144.

[80] P. K. Yeung and S. B. Pope. Lagrangian statistics from direct numerical simulations of isotropic turbulence. *J. Fluid Mech.*, 207:531, 2006.

[81] M. Mathur, G. Haller, T. Peacock, J. E. Ruppert-Felsot, and H. L. Swinney. Uncovering the Lagrangian skeleton of turbulence. *Phys. Rev. Lett.*, 98:144502, 2007.

[82] A. Arneodo, R. Benzi, J. Berg, L. Biferale, E. Bodenschatz, A. Busse, E. Calzavarini, B. Castaing, M. Cencini, L. Chevillard, R. Fisher, R. Grauer, H. Homann, D. Lamb, A.S. Lanotte, E. Leveque, B. Luethi, J. Mann, N. Mordant, W.-C. Mueller, S. Ott, N.T. Ouellette, J.-F. Pinton, S. B. Pope, S.G. Roux, F. Toschi, H. Xu, and P.K. Yeung. Universal intermittent properties of particle trajectories in highly turbulent flows. arXiv:0802.3776, 1989.

[83] Poul Olesen and Mogens H. Jensen. Exact periodic solutions of shells models of turbulence. arXiv:0705.3123, 2007.

[84] C.V. Abud and I.L. Caldas. On Slater's criterion for the breakup of invariant curves. *Physica D*, 308:34–39, 2015.

[85] G. A. Gottwald and I. Melbourne. A Huygens principle for diffusion and anomalous diffusion in spatially extended systems. *Proc. Natl. Acad. Sci.*, 110:8411–8416, 2013. arXiv:1304.3668.

[86] J. F. Gibson, J. Halcrow, and P. Cvitanović. Equilibrium and traveling-wave solutions of plane Couette flow. *J. Fluid Mech.*, 638:243–266, 2009. arXiv:0808.3375.

[87] A. Schmiegel. *Transition to turbulence in linearly stable shear flows*. PhD thesis, Philipps-Universität Marburg, 1999.

[88] J. F. Gibson. Database of invariant solutions of plane Couette flow. Technical report, Georgia Inst. of Technology, 2008. Channelflow.org/database.

[89] F. Waleffe. Homotopy of exact coherent structures in plane shear flows. *Physics of Fluids*, 15:1517–1543, 2003.

[90] P. Cvitanović, R. L. Davidchack, and E. Siminos. On the state space geometry of the Kuramoto-Sivashinsky flow in a periodic domain. *SIAM J. Appl. Dyn. Syst.*, 9:1–33, 2010. arXiv:0709.2944.

[91] J. M. Greene and J.-S. Kim. The steady states of the Kuramoto-Sivashinsky equation. *Physica D*, 33:99–120, 1988.

[92] A. M. Fox. A brief life and death of a torus: Computation of quasiperiodic solutions to the Kuramoto-Sivashinsky equation. In preparation, 2015.

[93] R. Paškauskas, C. Chandre, and T. Uzer. Bottlenecks to vibrational energy flow in OCS: Structures and mechanisms. *J. Chem. Phys.*, 130:164105, 2009.

[94] J. Porter and E. Knobloch. Dynamics in the 1:2 spatial resonance with broken reflection symmetry. *Physica D*, 201:318 – 344, 2005.

[95] S. Lange, M. Richter, F. Onken, A. Bäcker, and R. Ketzmerick. Global structure of regular tori in a generic 4D symplectic map. *Chaos*, 24, 2014.

[96] V. López, P. Boyland, M. T. Heath, and R. D. Moser. Relative periodic solutions of the Complex Ginzburg–Landau equation. *SIAM J. Appl. Dynam. Systems*, 4:1042–1075, 2006.

[97] P. S. Casas and À. Jorba. A numerical method for computing unstable quasi-periodic solutions for the 2-D Poiseuille flow. *International Conference on Differential Equations*, 2:884–886, 2000.

[98] D. Ruelle and F. Takens. On the nature of turbulence. *Commun. Math. Phys.*, 20:167, 1971.

[99] S. E. Newhouse, D. Ruelle, and F. Takens. Occurrence of strange Axiom A attractors near quasi-periodic flows on $T^m (m = 3$ or more). *Commun. Math. Phys.*, 64:35, 1978.

[100] Y. Lan and P. Cvitanović. Unstable recurrent patterns in Kuramoto-Sivashinsky dynamics. *Phys. Rev. E*, 78:026208, 2008. arXiv:0804.2474.

[101] A. P. Willis, P. Cvitanović, and M. Avila. Revealing the state space of turbulent pipe flow by symmetry reduction. *J. Fluid Mech.*, 721:514–540, 2013. arXiv:1203.3701.

[102] N. Fenichel. Persistence and smoothness of invariant manifolds for flows. *Indiana Univ. Math. J.*, 21:193–226, 1971.

[103] J.-L. Figueras and À. Haro. Reliable computation of robust response tori on the verge of breakdown. *SIAM J. Appl. Dyn. Syst.*, 11:597–628, 2012.